Title: Chemotherapy induces a YAP1-dependent fetal conversion to human Colorectal Cancer cells that is predictive of poor patient outcome

Authors: Laura Solé[1†], Teresa Lobo-Jarne[1†], Alberto Villanueva[2], Anna Vert[1], Yolanda Guillén[1], Irene Sangrador[1], Antonio Barbachano[3], Joan Lop[4], Marta Guix[5], Marta Salido[4], Beatriz Bellosillo[4], Raquel García-Romero[1], Marta Garrido[1], Jessica González[1], María Martínez-Iniesta[2], Erika Lopez-Arribillaga[1,6], Ramón Salazar[2], Clara Montagut[5], Ferrán Torres[7], Mar Iglesias[4], Toni Celià-Terrassa[1], Alberto Muñoz[3], Anna Bigas[1*] and Lluís Espinosa[1*].

Affiliations:

[1]Cancer Research Program, Institut Mar d'Investigacions Mèdiques, CIBERONC, Hospital del Mar, Barcelona 08003, Spain
[2]Translational Research Laboratory, Institut d'Investigació Biomèdica de Bellvitge (IDIBELL), Institut Català d'Oncologia, Hospitalet, Barcelona 08907, Spain.
[3]Department of Cancer Biology, Instituto de Investigaciones Biomédicas 'Alberto Sols', Spanish National Research Council (CSIC)-Autonomous University of Madrid (UAM) and IdiPAZ, CIBERONC, Madrid, Spain.
[4]Department of Pathology, Institut Mar d'Investigacions Mèdiques, Universitat Autònoma de Barcelona, CIBERONC, Barcelona 08003, Spain.
[5]Department of Oncology, Institut Mar d'Investigacions Mèdiques, CIBERONC, Universitat Pompeu Fabra, Barcelona 08003, Spain.
[6]Group of Biomedical Genomics, Institut de Recerca Biomedica (IRB), Barcelona 08028, Spain.
[7]Biostatistics and Data Management Platform, IDIBAPS, Hospital Clínic, Biostatistics Unit. Faculty of Medicine, Universitat Autònoma de Barcelona, Barcelona, Spain.

† Both first co-authors
* Corresponding authors

Mail to abigas@imim.es; lespinosa@imim.es

Abstract:

Current therapy against colorectal cancer is based on DNA-damaging agents that eradicate highly proliferative malignant cells. Whether sublethal chemotherapy affects tumor cell behavior and impacts on patient outcome is primarily unstudied. We now show that sublethal chemotherapy imposes a quiescent-like state to p53 wildtype human colorectal cancer (CRC) cells that is linked to the acquisition of a fetal phenotype downstream of YAP1, similar to that observed after intestinal damage. CRC cells displaying this fetal phenotype exhibit tumor-initiating activity comparable to untreated cells but superior metastatic capacity. Notably, nuclear YAP1 accumulation, or detection of the fetal signature in tumors predict poor prognosis in CRC patients carrying p53 wildtype tumors.

Collectively, our results uncover a potential adverse response of tumor cells to suboptimal chemotherapy, and identify nuclear YAP1 and fetal conversion of colorectal tumors as biomarkers for prognosis and therapy prescription.

Statement of significance:

Chemotherapy induces a quiescent-like phenotype to colorectal cancer cells that is linked to the acquisition of a YAP1-dependent fetal signature. Notably, this signature is predictive of patient outcome in different cohorts of human colorectal cancer.

INTRODUCTION

Colorectal cancer (CRC) remains the second leading cause of cancer-related death, which highlights the need for novel therapies focused on treatment of advanced disease. Treatment of localized CRC currently involves surgery, radiotherapy and/or chemotherapy (CT) (mainly 5-FU or capecitabine and oxaliplatin in the neoadjuvant or adjuvant setting), while CT (5-FU, oxaliplatin and irinotecan) still represents the main backbone of treatment for advanced CRC. In general, classical CT agents are designed to eradicate tumors by inducing DNA damage in highly proliferative cells leading to cell death (reviewed in (1)). However, most tumors contain a variable proportion of quiescent cells, including cancer stem cells, that are refractory to these agents thus contributing to tumor relapse and metastasis (2). In agreement with this notion, the presence of intestinal stem cell (ISC) signatures in tumors is predictive of poor prognosis in patients (3). Even after adequate treatment, around 25-30% of CRC patients in the less aggressive stage II tumors and up to 30-50% in stage III relapse and most of them eventually die (data from

the American Cancer Society). There is growing evidence that therapeutic strategies that potentiate the effect of DNA damaging agents may provide the base for more effective combination therapies (4,5).

Even when therapy fails to totally eradicate tumors, cancer cells receiving sublethal doses of therapeutic agents can acquire a senescent phenotype, characterized by high levels of the cell cycle inhibitors p16 and p21, cessation of proliferation and presence of a senescent-associated-secretory-phenotype (SASP) that effectively delays disease progression (6). However, senescent cells may still contribute to tumor progression as a source for relapse or metastasis, or by the secretion of pro-tumorigenic factors (reviewed in (7–9)). To date, there is an almost absolute lack of patient-based data to firmly establish the contribution of sub-lethal chemotherapy to patient outcome.

Recently, it was shown that fetal reprograming of intestinal cancer cells induced by YAP1 led to tumor and metastasis suppression in the Apc-/-; KrasG12D; p53-/- murine cancer model (10). We here show that p53 wildtype CRC patient-derived organoids (PDO)s treated with low doses of CT acquire a quiescent-like phenotype that is associated with YAP1-dependent fetal ISC conversion. These persistent quiescent-like (PQL) cells display high in vitro and in vivo tumor and metastasis initiating capacity, and we identified a restricted fetal ISC signature that is present in PQL cells and in a subset of untreated CRC tumors. Presence of this fetal signature or detection of nuclear YAP1 in tumors predicts poor disease outcome at stages II and III, in particular in CRC patients carrying tumors with functional p53 signaling.

RESULTS

Low-dose CT treatment of colorectal cancer PDOs induces a non-senescent quiescent phenotype in the absence of sustained DNA damage

To investigate the mechanisms that impose therapy resistant in cancer patients, we treated CRC PDOs with serial dilutions of the first-line CT agents 5-FU+Iri. Although high 5-FU+Iri. concentrations led to eradication of most PDO cells, we defined IC_{20} and IC_{30} as the 5-FU+Iri. doses that reduced cell viability by 20 and 30% after 72 hours of treatment, which were specific for each PDO (Figure 1A and Supplementary Table S1). Microscopy analysis of PDO5 (*TP53* WT) treated at IC_{20} and IC_{30} did not reveal obvious signs of cell death, but we noticed a dose-dependent growth arrest in all PDOs tested, that continued for at least 2 weeks after drug washout (Figures 1B and C, and S1A). Growth arrest was associated with inhibition of cell proliferation as determined by IHC analysis of ki67 (Figure 1D and S1B) and the reduced number of cells in S phase with accumulation in G_0/G_1 and G_2/M (Figure S1C), the latter probably corresponding to cells not undergoing cytokinesis (11,12). By fluorescent in-situ hybridization (FISH) and DAPI staining combined with IF of the membrane marker EPHB2, we demonstrated the absence of polyploid or multinucleated cells, respectively, following IC_{30} treatment (Figure S1D, E, F).

We determined whether IC_{20} and IC_{30} treatments inflicted a senescent phenotype to PDO5 cells by evaluation of senescence-associated (SA)-β-Galactosidase activity by flow cytometry (Figure 1E) and IHC (Figure S1G). Cells that persisted after IC_{20} or IC_{30} were not senescent, in contrast with cells treated at IC_{60} for 72 hours (Figure 1E). Accordingly, addition of the senolytic agent dasatinib (13) did not potentiate the growth inhibition imposed by IC_{20} and IC_{30} 5-FU+Iri. but enhanced the effect of IC_{60} 5-FU+Iri. treatment (Figure 1F). Moreover, we did not detect apoptotic PDO5 cells after IC_{30} treatment as determined by cleaved-caspase 3 staining (Figure S1H) and Annexin V staining (Figure S1I). We studied the possibility that cell cycle arrest after IC_{20} and IC_{30} treatment was linked to sustained DNA damage. Comet assay (Figures 1G) and WB analysis of the γH2A.X marker (Figure 1H) in PDO5 revealed a dose-dependent accumulation of DNA damage starting at 1-3 hours with a maximum at 24 hours. Importantly, DNA damage was undetectable at 72 hours after IC_{20} and IC_{30} treatment, but clearly present in IC_{60}-treated PDO5 (Figure 1H and 1I). In contrast, PDO4 and PDO8 cells carrying mutated *TP53* exhibited high amounts of DNA damage following IC_{20} and IC_{30} 5-FU+Iri. treatment that lasted for at least 72 hours (Figure 1J), in agreement with the higher growth inhibition of *TP53* mutant PDOs after CT washout (Figure S1A).

These results indicate that p53 wildtype cancer cells that persisted after low CT acquire a quiescent-like phenotype, hereafter referred as PQL (for persistent quiescent-like), in the absence of sustained DNA damage.

CT-induced PQL cells display fetal intestinal stem cells (feISC) characteristics

Sublethal CT treatment has been linked to the acquisition of specific stem cell signatures in B-cell lymphoma (8) and intestinal cancer (14). To study the transcriptional changes associated

with the PQL phenotype, we performed RNA sequencing (RNA-seq) of control, IC_{20}- and IC_{30}-treated PDO5 cells. Bioinformatic examination of differentially expressed genes (DEGs) (Supplementary Table S2) showed an almost perfect correlation of gene expression changes between pairwise comparisons (IC_{20} vs. untreated and IC_{30} vs. untreated) ($p<2.2e-16$, $R=0.974$) (Figure S2A). Gene Set Enrichment Analysis (GSEA) uncovered p53 as the main activated pathway in PQL cells (Figure 2A), which was confirmed by WB analysis (Figure 2B), qPCR (Figure 2C) and ChIP assay (Figure S2B) of canonical p53 targets. DEGs genes also clustered in the NF-κB, epithelial-to-mesenchymal transition (EMT) and interferon gamma (IFNγ) pathways (Figure 2A) that have been associated with inflammatory response and stemness (15–19). Unexpectedly, DEG in our analysis negatively correlated with a canonical ISC signature (Muñoz et al., 2012) (Figure 2D). More in-depth analysis showed a mixed pattern of genes up-regulated such as *LY6D* and *YAP1*, which are instrumental in the fetal ISC (feISC) after intestinal injury (10,19–21), and down-regulated such is the case of canonical adult ISC markers *LGR5* and *EPHB2* (Figure 2E). Accordingly, GSEA indicated a significant correlation between the CT-induced signature and the transcriptional program associated with fetal ISC conversion (21) (Figure 2F and 2G).

The feISC signature shows a coordinate expression in human CRC and is dependent of functional p53

We asked whether CT-induced feISC signature was present in untreated human tumors. Computational analysis of the Marisa (22) (GSE39582), Jorissen (23) (GSE14333) and TCGA (TCGA Portal) CRC datasets using CANCERTOOL (24) indicated that many genes of the signature were distributed in clusters of coordinate expression in untreated tumors (with either positive or negative correlation) (supplementary Table S3), which we integrated in a new cluster containing 28 plus 8 genes that were either upregulated (28up) or downregulated (8down) in CT-treated PDOs and fetal-converted ISCs (Figure S3A). This new 28up+8down-feISC gene signature was present in Marisa (Figure 3A), Jorissen and TCGA CRC cohorts (not depicted). We confirmed regulation of several genes of the 28up+8down-feISC signature by RT-qPCR (Figure 3B) and WB analysis (Figure 3C) of IC_{20} 5-FU+Iri.-treated PDO5. Activation of fetal genes following CT treatment was comparably observed in the *TP53* WT PDO66 (Figure 3D) but significantly impaired in the hypomorphic *TP53* mutant PDO4 (Figure 3E). We confirmed the p53 dependency of the feISC signature through generation by CRISPR-Cas9 of PDO5 pools with variable degrees of p53 KO (Figure S3B). RT-qPCR analysis revealed that PDO5 KO#3 with the highest p53 KO efficiency showed lower activation of 28up-feISC genes after 5-FU+iri. IC_{20} treatment (Figure 3F). However, we only detected slight differences in the protein levels of randomly selected fetal markers when comparing CRC cell lines carrying WT or mutant p53, with the latter showing a massive accumulation of the DNA damage marker γH2A.X after CT (Figure 3G). ChIP-seq assay of 5-FU+Iri. IC_{20}-treated PDO5 cells indicated that only 3 genes in the 28up-feISC signature, PLK2, PHLDA3 and GSN genes were direct p53 targets (Figure

S3C), consistent with previously published data (25). These results suggested that additional transcription factor/s govern fetal ISC conversion by CT.

We also determined whether untreated tumors carrying the 28up+8down-feISC signature were restricted to a specific molecular cancer subtype. 74% of tumors with the 28up+8down-feISC signature were categorized as CSM4, based on the classification by Guinney and collaborators (26) (Figure 3H), which is characterized by upregulation of epithelial to mesenchymal transition gene signatures, TGFβ signaling, stromal infiltration and poorer patient prognosis. In contrast, 28up-low+8down-high tumors were primarily ascribed to the more canonical Wnt and Myc-driven CMS2 subtype. We studied whether the feISC signature of untreated tumors was expressed in the epithelial cancer cells or primarily contributed by the stromal component. Analysis of single cell RNA-seq data from Lee and collaborators (27) demonstrated that feISC genes are expressed in the epithelial cancer cells, particularly in states 1, 5 and 6 that are all associated with the secretory and migratory pathways (Figure 3I).

These results indicate that sublethal CT induces a fetal signature, which is dependent on the presence of a functional p53 pathway. This feISC signature is also expressed in a coordinate manner in untreated human CRC tumors, in particular in tumors of the CMS4 subtype from Guinney and collaborators, and the secretory and migratory epithelial states 1, 5 and 6 from Lee and collaborators.

PQL cancer cells display increased in vitro and in vivo tumor initiation capacity.

It was recently shown that fetal ISC conversion imposed by YAP1 activation (induced by deletion of the Hippo kinases LATS1/2) in the $Apc^{-/-}$; $Kras^{G12D}$; $p53^{-/-}$ murine intestinal tumor cells results in tumor and metastasis suppression (10). Thus, we studied whether p53 proficient PQL cells, which display a consistent activation of a feISC signature, preserved tumor initiation capacity (TIC) of untreated cancer cells. We seeded 300 single cells from untreated or 5-FU+Iri. IC_{20} or IC_{30}-treated PDO5, as indicated. We found that CT pretreatment of PDO5 cells did not affect their TIC in vitro compared with untreated cells, as indicated by the equivalent number of spheres generated (Figures 4A, upper panel), but imposed a dose-dependent reduction of spheres diameter (Figures 4A, lower panel), consistent with their low proliferation rates. In contrast, 5-FU+Iri. pretreatment (IC_{20}) of *TP53* mutant PDO4 and PDO8 cells resulted in TIC abrogation (Figure 4B), which is in agreement with the massive accumulation of DNA damage detected in comet assays (see Figure 1J). Considering that TIC activity in PDO5 could be driven by the fraction of cells which still undergo replication after IC_{20} and IC_{30} treatment (Figure 1D, S1B and S1C), we next compared the TIC in vitro of the general population and specifically the quiescent cells. For this, we generated *TP53* WT PDO5 carrying a doxycycline-inducible histone-GFP reporter that has been previously demonstrated to label the quiescent tumor population after doxycycline withdrawal (28). Upon 6 days of doxycycline treatment, PDO5 cells were treated

with 5-FU+Iri. for 72 hours and, after 2 weeks of doxycycline washout, analyzed by flow cytometry and GFP_{high} and GFP_{low} were sorted (S4A). We found that sorted GFP_{high}, which represents the quiescent population of CT-treated cells, displayed identical capacity for organoid generation as GFP_{high} plus GFP_{low} cells indicating that TIC activity is retained in the PQL population.

We next studied the in vivo tumorigenic capacity of IC_{20} and IC_{30} pretreated PDO5 cells using two complementary strategies. Firstly, we performed intracardiac injection of 40.000 single PDO5 cells (untreated, IC_{20} or IC_{30} pretreated) labelled with firefly luciferase into NOD-SCID-gamma (NSG) immunocompromised mice. Mice were analyzed weekly using bioluminescence (BLI) to monitor metastatic growth using the IVIS animal imaging system (Figure 4C). We found that PDO5 treated with 5-FU+Iri. displayed a slightly superior metastatic capacity than untreated cells. Specifically, 4 of 8 mice transplanted with untreated PDO5 cells contained metastatic lesions at week 15 after transplantation. Importantly, 4 of 6 mice transplanted with IC_{20}-treated cells and 5 of 6 mice with IC_{30}-treated cells showed visible metastasis 15 weeks after injection (Figure 4D and 4E). Secondly, we inoculated equivalent numbers of untreated, IC_{20} and IC_{30} pretreated PDO5 cells in the cecum of nude mice. Tumor growth was assessed by palpation weekly and animals sacrificed synchronously 70 days after transplantation. We found that untreated, IC_{20} and IC_{30}-treated PDOs all generated tumors in the site of inoculation, being IC_{20} and IC_{30}-treated derived tumors being much smaller than those arising from untreated controls (Figure 4F), as expected. Importantly IC_{20} and IC_{30}-treated PDO cells displayed a significantly higher ability to generate intraperitoneal implants when compared with untreated tumor cells (Figure 4G and 4H). Still, we detected a reduction in the proliferation capacity of CT-treated PDO5 cells as determined by IHC analysis of the proliferation marker ki67 (Figure 4I).

These results indicate that *TP53* WT CRC cells treated with low doses of 5-FU+Iri. show reduced capacity to proliferate in vitro and in the primary tumors, but display comparable TIC as untreated cells in vitro and higher metastatic activity in vivo.

The CT induced feISC signature is predictive of reduced disease-free survival in *TP53* WT tumors

We studied the possibility that the presence of the feISC signature in untreated CRC tumors was associated with patients' outcome. To this aim, we analyzed the predictive capacity of the 28up+8down-feISC gene signature in the Marisa, Jorissen and TCGA CRC data sets. The global 28up+8down-feISC signature was sufficient to demarcate at least 2 subsets of patients in either data set (Figure 5A and Supplementary Table S4), with the group with highest 28up and lowest 8down-feISC levels displaying the poorest disease-free-survival (Figure 5B). A more detailed analysis of the Marisa data set demonstrated that this signature was significantly associated with tumor relapse in patients at stages II (n=264) (p=0.041) (Figure 5C) and II+III (n=469)

(p=0.0033) (Figure 5C and 5D), and imposed a trend towards poor prognosis at stage IV (n=60) (Figure 5E).

Since presence of functional p53 defined feISC conversion and TIC maintenance (see Figures 3F, 4A and 4B), we explored the possibility that *TP53* status determined the prognosis value of 28up+8down-feISC signature in CRC patients. Stratification of Marisa (Figure 5F) and TCGA (Figure S5A) patients according to *TP53* status did not have prognosis value by itself, but determines the prognosis value of 28up+8down-feISC signature (Figures 5G and Figure S5B). Because 28up+8down-feISC tumors are mainly included in the worst prognosis CMS4, we tested whether this feISC signature represents an independent prognosis factor inside this molecular subtype. Our results indicate that the 28up+8down-feISC signature increased the risk of relapse in patients within the CMS4 group (Figure 5H).

Finally, we explored the possibility of identifying a simplified signature derived from the 28up+8down-feISC with comparable prognosis value in cancer, which would facilitate its implantation in the clinical practice. We scored genes by their coordinate expression in the 3 CRC datasets analyzed (supplementary Table S5). Then we evaluated the added value of single genes to the simplest signature composed by the highest scored 28up plus the highest scored 8down-feISC gene. We uncovered a minimal 5up+3down-feISC signature that shared coordinate expression in tumors (Figure S5C) and stratified patients with poor prognosis in all tested CRC cohorts (Marisa, p=0.00003; Jorissen, p=0.0002; TCGA, p=0.037) (Figure S5D) including patients carrying tumors at stage II and II-III (Figure 5I).

Acquisition of feISC by CT treatment is linked to and dependent on YAP1 activation

We investigated whether feISC conversion of CRC cells after CT treatment was YAP1 dependent, as previously found in mouse models (10,20). WB analysis of PDO5 cells (Figure 6A) and various CRC cell lines (Figure 6B) showed increased YAP1 expression after 5-FU+Iri. treatment, that was restricted to cells carrying WT *TP53* (Figure 6B). We detected accumulation of nuclear (active) YAP1 in IC_{20} and IC_{30}-derived PDO5 tumors at 2 months after implantation in mice (Figure 6C). Next, we studied whether YAP1 activity was required for transcriptional induction of feISC genes by CT. Incubation of PDO5 cells with the YAP1 inhibitor verteporfin precluded induction of all tested feISC genes following IC_{20} 5-FU+Iri. treatment (Figure 6D). Similarly, IC_{20} 5-FU+Iri. treatment of Ls174T CRC cells led to an increase in YAP, SERPINH1 and TSPAN4 protein levels, which was abrogated by verteporfin (Figure S6A). Importantly, verteporfin alone, but more effectively in combination with CT, promotes tumor cell death in both *TP53* WT and *TP53* mutant PDO cells (Figures 6E). In addition, we observed that IC_{20} and IC_{30} pre-treated PDO cells show increased resistance to subsequent CT treatment (Figure S6B) that was prevented by addition of verteporfin (Figure 6F) strongly suggesting that combination of CT plus YAP1 inhibitors may represent a suitable therapeutic strategy for eradicating CRC tumors showing fetal ISC conversion.

Then, we performed IHC analysis of ki67 (to determine the proliferation status) and YAP1 in 62-paired human CRC tumors collected at diagnosis (biopsy) and after DNA damaging-based neoadjuvant treatment (surgery). Whereas some tumors exhibited similar proliferation rates after treatment, as determined by Ki67 staining (type 1), we identified a large subset of tumors that displayed reduced proliferation with no morphological evidences of senescence (type 2), such as enlarged nuclei or expression of the senescence marker p16 (Figure S6C), which are observed in scarce tumors at surgery (type 3) (Supplementary Table S6). We failed to detect differences in patient prognosis when comparing type 1 and type 2 tumors that are readily observed in patient carrying type 3 tumors (no events of relapse in the follow-up period) (Figure S6D). Interestingly, we detected nuclear YAP1 in few epithelial cells of untreated tumors, which was massively increased in neoadjuvant treated tumors independently of the proliferation status (Figure 6G and Supplementary Table S6), associated with expression of the feISC markers S100A4 and SERPINH1 (Figure 6H).

Since the number of samples in the studied cohort was insufficient to evaluate the clinical impact of nuclear YAP1 accumulation, we performed IHC analysis of YAP1 in a tissue microarray containing 196 different human CRC samples in triplicates with available clinical data. We determined the H score of nuclear YAP1 (as intensity multiplied by percent of positive tumor cells) in the triplicates and stratified the CRC patients accordingly. Considering the mean value ± 0.2 standard deviations of the H-score, we observed a trend towards poor prognosis in the group with higher nuclear YAP1 (disease-free survival: p=0.26; HR=1.38, not depicted) that increased when considering mean value ± 0.4 s.d. (p=0.12; HR=1.58, not depicted). Importantly, nuclear YAP1 levels reached statistical significance when considering the mean value ± 0.6 standard deviations (p=0.039; HR=1.97) (Figure 6I and 6J).

Together our data indicate that sublethal CT promotes the conversion of tumor cells into a fetal ISC phenotype that favors cancer progression and metastasis. Moreover, we uncover a CT-induced 28up+8down-feISC signature and its derivative the 5up+3down-feISC signature, which are present in a subset of untreated CRC tumors and has prognosis value in the context of functional p53. Finally, we demonstrated the higher efficacy of CT in combination with YAP1 inhibitors for eradication of *TP53* WT tumors, and the possibility of using nuclear YAP1 detection to identify patients that could benefit from this therapeutic strategy.

DISCUSSION

CT is the current treatment for advanced and metastatic colorectal tumors. However, in a percent of cases tumor cells that escape from death imposed by therapeutic drugs (by efficient drug clearance, effective DNA repair or due to reduced accessibility of the drugs to specific tumor areas) can acquire a dormant phenotype that provides superior resistance to subsequent DNA damaging-based treatment based on their less proliferative state. In the present study we have shown that sublethal doses of CT impose a non-senescent and non-proliferating phenotype to cancer cells, in the absence of persistent DNA damage. Although discriminating between senescence and quiescence is not essential, since senescence was demonstrated to be reversible depending on the alternative use of p53/p21 (reversible) or p16/RB (irreversible) (29) leading to increased tumor stemness (8), we unequivocally observed that CT-treated cells display a quiescence-like state in the absence of a robust senescence phenotype. Importantly, PQL cancer cells can efficiently escape from dormancy following in vivo transplantation, as it is shown in the xenograft experiments, displaying a superior capacity to escape from the site of implantation. This is in agreement with the higher metastatic potential observed for CT treated cells and in line with previously studies showing that dormant cell populations in primary human CRC cells still retains tumor propagation potential (30) and that specific subpopulations of cancer cells reversibly enter a quiescent state and exhibit increased tumorigenic potential in response to CT (31).

Our transcriptomic studies revealed that the dynamics associated with the acquisition of the PQL phenotype rely downstream of p53 and p21 signaling. It has long been established that the key regulatory proteins that mediate cell cycle block include p53, p21 and p16, among others (reviewed in (32). The finding that the cancer cells carrying dysfunctional p53 did not acquire the PQL phenotype but display massive amounts of DNA damage may explain the results obtained by Cheung and collaborators indicating that YAP1 activation acts as tumor suppressor in p53 depleted tumors (10). In this context, our results are of particular relevance since they clarify the functional contribution of YAP1 as driver of fetal conversion and metastasis in p53 WT colorectal cancer, which is in agreement with previous reports (reviewed in (33)). In the same direction, it has been recently demonstrated that tumor cells that resist prolong CT acquire an embryonic-like and quiescent state that facilitates therapeutic resistance (34). We propose that functional p53 through p21 upregulation imposes a stop in proliferation when exposed to low CT doses that allow cells to recover under specific conditions, whereas cell depleted of functional p53 continue proliferating thus accumulating irreparable damage and apoptotic death. This cellular response represents, in fact, a double-edge sword since it can impose specific outcomes depending on the *TP53* status and the heterogeneity of cancer cells. In this sense, it was demonstrated that 5-FU treatment induced cell dormancy and epithelial to mesenchyme

transition in lung cancer cells, associated with p53 accumulation (35). Further experiments genetically deleting YAP1 in *TP53* WT cells and preclinical assays using YAP1 inhibitors are required to definitively demonstrate the possibility of using specific protocols to combat fetal-converted tumors.

Remarkably, we have shown that the sublethal CT-induced feISC signature is already present in a subset of untreated tumors at diagnosis in several CRC cohorts. It is tempting to speculate that extrinsic factors or non-cancer cells present in the tumor, such as inflammatory cells, may induce the upstream regulators of this signature (i.e., TGFβ signaling) thus leading to the acquisition of PQL traits in the absence of treatment. In agreement with this idea, tumors carrying the 28up+8down-feISC signature are primarily included in the CMS4 CRC subtype identified by Guinney and collaborators (26) and characterized by stromal infiltration and TGFβ signaling. We speculate that TGFβ or additional cytokines derived from the tumor stroma may impose a YAP1-dependent feISC signature, which is in agreement with the previous demonstration that TGFβ promotes YAP1 signaling by facilitating the degradation of the negative regulator of the pathway RASSF1A (36). To recognize patients with higher probability of recurrence among those of uncertain prognosis (stages II-III) by the analysis of a reduced feISC signature can be clinically relevant as it may suggest more aggressive treatments or to intensify patient follow-up. Additionally, targeting the upstream signals imposing PQL/feISC acquisition pharmacologically (i.e. YAP1 inhibitors) or using combination treatments that effectively eradicate quiescent tumor cell populations (i.e. CT plus inhibitors of the NHEJ repair pathway) appear as interesting therapeutic options.

On the other hand, we identified IFN signaling in the analysis of CT-induced genes associated with PQL acquisition, which is in agreement with the essential function of IFN pathway in the conversion of adult stem cells into a fetal ISC phenotype (19). Conversion of adult into fetal ISC had already been identified as part of the process of tissue regeneration after helminths infection (19) or in the Dextran Sulfate Sodium colitis model (20). Thus, our results reinforce the concept that tumor development is partially mimicking the tissue regeneration process.

Our findings linking fetal ISC conversion poor CRC prognosis are partially in contrast with data indicating the prognosis factor of the adult ISC signature, including Lgr5 (3). Nevertheless, it has been recently demonstrated that Lgr5 and other adult ISC markers are temporary lost from cells seeding metastases, and subsequently recovered (due to cellular plasticity) to allow metastasis establishment (37) and most data indicating the requirement for adult Lgr5+ ISC in metastasis seeding have been obtained on p53-deficient tumor cells (10,38). Interestingly, Batlle's group recently identified a different contribution of Lgr5+ cells in PDOs carrying mutated or WT *TP53* (higher in mutant *TP53*) (39) thus opening the possibility that dependance on adult Lgr5+ ISCs for cancer progression is linked to *TP53* deficiency, which should be further investigated. Independently on the mechanisms underlying conversion of adult into fetal ISCs (induced by CT

418 or signals derived from the tumor stroma), we have here identified a restricted genetic signature
419 that is present in a subset of tumors that are mostly included in the CMS4 (the cancer stem cell
420 and poor prognosis subtype) but clearly differ from that of adult ISCs.
421
422 From a clinical perspective, uncovering genetic signatures that are predictive of recurrence in a
423 group of patients with uncertain projection (stages II and III) will represent a powerful tool for
424 diagnosis refinement. In this direction, we are currently setting up the protocols for early
425 detection of PQL/feISC cells in stages II-III tumors at diagnosis. As mentioned, anticipating the
426 presence of this adverse phenotype in tumors would allow exposing selected groups of patients
427 to alternative therapeutic procedures that could be refined with the discovery of the mechanisms
428 imposing fetal SC conversion in cancer.
429
430
431

METHODS

Study design

The goal of this study was to determine in patient-derived data that chemotherapy positively or negatively impact on colorectal cancer progression in case of incomplete remission. Study of sublethal doses of DNA-damaging agents was performed in several patient-derived organoids and human cell lines to demonstrate its broad effects. By taking advantage of public colorectal tumor databases, the expression profiling of genetic signatures was accomplished. The numbers of experiments, biological replicates, and sample sizes for each database are outlined in the figure legends.

Reagents, antibodies and software

A table of the source of all reagents, antibodies, kits, cell lines, chemicals and software is included (Table S8).

Animal studies

Fragments of human colorectal tumors obtained from Parc de Salut MAR Biobank (MARbiobank) with the informed consent of patients and following all recommendations of Hospital del Mar' Ethics Committee, the Spanish regulations, and the Helsinki declaration's Guide were transplanted and expanded in the cecum of nude mice as orthoxenografts. To perform tumor-initiating assays, two approaches were used. Firstly, intracardiac injection of 40.000 CT (n=8) and IC_{20} (n=7) or IC_{30} (n=6) -treated PDO5 cells carrying a luciferase reporter to NSG mice was performed. For checking that the injection was performed correctly, after injection animals were anesthetized and were given 100µl of substrate D-luciferin at 15 mg/ml by intraorbital injection. Bioluminescent imaging was performed placing the animals into the IVIS Lumina III In Vivo Imaging System (PerkinElmer). Images were recorded with an exposure time of 2 minutes and were taken every week. Quantification was done using Living Image® software (PerkinElmer). Secondly, equivalent amounts of disaggregated patient-derived organoids (PDOs), previously treated as indicated below, were implanted as orthoxenografts. Follow-up of the growing tumors was done by palpation and animals were sacrificed when controls developed tumors of around 2 cm of diameter. In all our procedures, animals were kept under pathogen-free conditions, and animal work was conducted according to the guidelines from the Animal Care Committee at the Generalitat de Catalunya. The Committee for Animal Experimentation at the Institute of Biomedical Research of Bellvitge (Barcelona) approved these studies.

Patient-derived organoids and culture conditions

Samples from patients were kindly provided by MARBiobank and IdiPAZ Biobank, integrated in the Spanish Hospital Biobanks Network (RetBioH; www.redbiobancos.es). Informed consent was obtained from all participants and protocols were approved by institutional ethical committees. For patient-derived organoids (PDOs) generation, primary or xenografted human

colorectal tumors were disaggregated in 1.5 mg/mL collagenase II and 20 µg/mL hyaluronidase after 40min of incubation at 37ºC, filtered in 100 µm cell strainer and seeded in 50 µL Matrigel in 24-well plates, as previously described (40). After polymerization, 450 µL of complete medium was added (DMEM/F12 plus penicillin (100 U/mL) and streptomycin (100 µg/mL), 100 µg/mL Primocin, 1X N2 and B27, 10mM Nicotinamide; 1.25 mM N-Acetyl-L-cysteine, 100 ng/mL Noggin and 100 ng/mL R-spondin-1, 10 µM Y-27632, 10 nM PGE2, 3 µM SB202190, 0.5 µM A-8301, 50 ng/mL EGF and 10 nM Gastrin I). Tumor spheres were collected and digested with an adequate amount of trypsin to single cells and re-plated in culture. Cultures were maintained at 37°C, 5% CO_2 and medium changed every week. PDOs were expanded by serial passaging and kept frozen in liquid Nitrogen for being used in subsequent experiments. Mutations identified in the PDOs are listed in Supplementary Table S1.

Cell lines

CRC cell lines HCT116 and Ls174T (*KRAS* mutated and *TP53* WT), SW480 (*KRAS* and *TP53* mutated) and HT29 (B*RAF* and *TP53* mutated) were obtained from the American Type Culture Collection (ATCC, USA). All cells were grown in Dulbecco's modified Eagle's medium (Invitrogen) plus 10% fetal bovine serum (Biological Industries) and were maintained in a 5% CO_2 incubator at 37°C. 5-FU+Iri. concentrations that reduced 30% of each cell growth were as follows: HCT116, 0.01 µg/mL 5-FU and 0.004 µg/mL Iri.; Ls174T, 0.025 µg/mL 5-FU and 0.01 µg/mL Iri.; SW480, 0.28 µg/mL 5-FU and 0.11 µg/mL Iri.; HT29, 0.33 µg/mL 5-FU and 0.13 µg/mL Iri.

Human colorectal cell lines

Formalin-fixed, paraffin-embedded tissue blocks of gastrointestinal tumor samples, from patients at diagnosis and after neoadjuvant therapy at the time of surgery, were obtained from Parc de Salut Mar Biobank (MARBiobank, Barcelona). Samples were retrieved under informed consent and approval of the Tumor Bank Committees according to Spanish ethical regulations and the guidelines of the Declaration of Helsinki. Patient identity for pathological specimens remained anonymous in the context of this study. Patient data was collected (Supplementary Table S6). IHC analyses were performed as described below.

Patient-derived organoids viability assays

600 single PDO cells were plated in 96-well plates in 10 µL Matrigel with 100 µL of complete medium. After 6 days in culture, growing PDOs were treated with combinations of 5-FU+Iri. for 72 hours at the concentrations that reduce a 20 and 30% of the cell growth (IC_{20} and IC_{30}, respectively), which are specific for each PDO as described in Supplementary Table S1. After 72 hours of treatment, we changed to fresh medium and measured the cell viability after 3 days, 1 week and 2 weeks using the CellTiter-Glo 3D Cell Viability Assay following manufacturer's instructions in an Orion II multiplate luminometer. Images were obtained with an Olympus

BX61 microscope at the indicated time points and the diameter of at least 70 tumoroids per condition was determined using Adobe Photoshop. For dose-response curves, PDOs were plated in 96-well plates in Matrigel and after 6 days in culture were treated with combinations of 5-FU and Irinotecan. Following 72 hours of treatment, we changed to fresh medium and treated with increasing concentrations of either 5-FU+Iri., dasatinib, verteporfin or combinations for 72 hours at the indicated concentrations. Cell viability was determined as described.

Cell cycle analysis.

Cell cycle was determined by flow cytometry using the standard APC BrdU Flow Kit. Briefly, treated PDOs with combinations of 5-FU+Iri., as indicated, were stained with bromodeoxyuridine (BrdU) for 24 hours. Single cells were obtained and processed according to the manufacturer's instructions, with DAPI staining for the DNA content. The cells were analyzed in the LSR II analyzer.

Cell senescence assays

Cell senescence was identified by the presence of SA-β-galactosidase activity using two different approaches. On one hand, staining for SA-β-galactosidase activity in cultured cells was carried out using the Senescence β-Galactosidase Staining Kit. Briefly, PDOs were seeded in 24-well plates (3000 cells per well). After 6 days, PDOs were treated with combinations of 5-FU+Iri. for 72 hours and were subsequent stained with the β-Galactosidase Staining Solution for 2 hours, according to the manufacturer's instructions. Sections embedded in paraffin were counterstained with Fast Red for nuclei visualization. Images were obtained with an Olympus BX61 microscope. On the other hand, SA-β-galactosidase activity was addressed by flow cytometry using the Cell Event Senescence Green Flow Cytometry Assay Kit following the manufacturer's instructions, and analyzed in the LSR II analyzer.

Cell lysis and Western Blot

Treated PDOs were lysed for 20 min on ice in 300 µL of PBS plus 0.5% Triton X-100, 1 mM EDTA, 100 mM NA-orthovanadate, 0.2 mM phenyl-methylsulfonyl fluoride, and complete protease and phosphatase inhibitor cocktails. Lysates were analysed by western blotting using standard SDS–polyacrylamide gel electrophoresis (SDS-PAGE) techniques. In brief, protein samples were boiled in Laemmli buffer, run in polyacrylamide gels, and transferred onto polyvinylidene difluoride (PVDF) membranes. The membranes were incubated with the appropriate primary antibodies overnight at 4ºC, washed and incubated with specific secondary horseradish peroxidase–linked antibodies. Peroxidase activity was visualized using the enhanced chemiluminescence reagent and autoradiography films.

RT-qPCR analysis

Total RNA from treated PDOs was extracted with the RNeasy Micro Kit, and cDNA was produced with the RT-First Strand cDNA Synthesis Kit. RT-qPCR was performed in LightCycler 480 system using SYBR Green I Master Kit. Samples were normalized to the mean

552 of the housekeeping genes *TBP* and *HPRT1*. Primers used for RT-qPCR are listed in
553 Supplementary Table S7.
554
555 **ChIP-sequencing analysis**
556 IC20-treated PDO5 was subjected to ChIP as previously described (41). Briefly, formaldehyde
557 crosslinked cell extracts were sonicated, and chromatin fractions were incubated for 16 h with
558 anti-p53 [abcam ab 1101] antibody in RIPA buffer and then precipitated with protein A/G-
559 sepharose [GE Healthcare, Refs. 17-0618-01 and 17-0780-01]. Crosslinkage was reversed, and
560 6–10 ng of precipitated chromatin was directly sequenced in the genomics facility of Parc de
561 Recerca Biomèdica de Barcelona (PRBB) using Illumina® HiSeq platform. Raw single-end 50-
562 bp sequences were filtered by quality (Q > 30) and length (length > 20 bp) with Trim Galore
563 (42). Filtered sequences were aligned against the reference genome (hg38) with Bowtie2 (43).
564 MACS2 software (44) was run first for each replicate using unique alignments (q-value < 0.1).
565 Peak annotation was performed with ChIPseeker package (45) and peak visualization was done
566 with Integrative Genomics Viewer (IGV). ChIP- sequencing data are deposited at the GEO
567 database with accession number GSE164161.
568
569 **RNA-sequencing experiments and data analysis**
570 Total RNA from untreated and treated PDOs was extracted using RNeasy Micro Kit. The RNA
571 concentration and integrity were determined using Agilent Bioanalyzer [Agilent Technologies].
572 Libraries were prepared at the Genomics Unit of PRBB (Barcelona, Spain) using standard
573 protocols, and cDNA was sequenced using Illumina HiSeq platform, obtaining ~ 45-64 million
574 50-bp paired□end reads per sample. Adapter sequences were trimmed with Trim Galore.
575 Sequences were filtered by quality ($Q > 30$) and length (> 20 bp). Filtered reads were mapped
576 against the latest release of the human reference genome (hg38) using default parameters of
577 TopHat (v.2.1.1) (46) and expressed transcripts were then assembled. High-quality alignments
578 were fed to HTSeq (v.0.9.1) (47) to estimate the normalized counts of each expressed gene.
579 Differentially expressed genes between different conditions were explored using DESeq2 R
580 package (v.1.24.0) (48) and adjusted P-values for multiple comparisons were calculated applying
581 the Benjamini-Hochberg correction (FDR) (see Supplementary Table S2). Plots were done in R.
582 Expression heatmaps were generating using the heatmaply and pheatmap packages in R (49).
583 Gene Set Enrichment Analysis (GSEA) was performed with described gene sets using gene set
584 permutations (n = 1000) for the assessment of significance and signal-to-noise metric for ranking
585 genes. RNA-sequencing data are deposited at the GEO database with accession number
586 GSE155354.
587
588 **Signature definition**
589 To generate the fetal intestinal stem cell signatures, we selected genes with log2 Fold Change
590 (FC) TreatedvsControl > 0 and FetalvsAdult (21) > 0 in the case of the 28up-feISC and $\log^2$FC
591 TreatedvsControl < 0 and FetalvsAdult < 0 in the case of the 8down-feISC. Next, we used the

Marisa data set to performed expression correlation matrices for the selected expression gene pairs using the corrplot package (v.0.84). To obtain the simplified signature genes were scored by their coordinate expression taking into account the three CRCR datasets analyzed (see Supplementary Table S5). Then it was evaluated adding a value of single genes to the simplest signature composed by the highest scored 28up plus the highest scored 8down-feISC. The process ended when adding a gene did not improved the prognosis value. Correlations were considered as statistically significant when the Pearson correlation coefficient corresponded to a p value below 0.05. Clusters of genes were selected when the absolute value for the Pearson correlation coefficient was above 0.1. Correlations were considered as statistically significant when the Pearson correlation coefficient corresponded to a p value below 0.05. Clusters of genes were selected when the absolute value for the Pearson correlation coefficient was above 0.1.

Quantification and Statistical analysis

Statistical parameters, including number of events quantified, standard deviation and statistical significance, are reported in the figures and in the figure legends. Statistical analysis has been performed using GraphPad Prism 6 software, and $P < 0.05$ is considered significant. Two-sided Student's t-test was used to compare differences between two groups. Each experiment shown in the manuscript has been repeated at least twice. Combinations of 5-FU+Iri. treatment has been checked for an appropriate IC20 and IC30 effect in every experiment, by cell viability assay. Bioinformatic analyses were performed as indicated above.

REFERENCES

1. Brenner H, Kloor M, Pox CP. Colorectal cancer. Lancet. 2014.
2. Batlle E, Clevers H. Cancer stem cells revisited. Nat. Med. 2017.
3. Merlos-Suárez A, Barriga FM, Jung P, Iglesias M, Céspedes MV, Rossell D, et al. The intestinal stem cell signature identifies colorectal cancer stem cells and predicts disease relapse. Cell Stem Cell. 2011;
4. Colomer C, Margalef P, Villanueva A, Vert A, Pecharroman I, Solé L, et al. IKKα Kinase Regulates the DNA Damage Response and Drives Chemo-resistance in Cancer. Mol Cell. 2019;75.
5. Cánovas B, Igea A, Sartori AA, Gomis RR, Paull TT, Isoda M, et al. Targeting p38α Increases DNA Damage, Chromosome Instability, and the Anti-tumoral Response to Taxanes in Breast Cancer Cells. Cancer Cell. 2018;
6. He S, Sharpless NE. Senescence in Health and Disease. Cell. 2017.
7. Faget D V., Ren Q, Stewart SA. Unmasking senescence: context-dependent effects of SASP in cancer. Nat. Rev. Cancer. 2019.
8. Milanovic M, Fan DNY, Belenki D, Däbritz JHM, Zhao Z, Yu Y, et al. Senescence-associated reprogramming promotes cancer stemness. Nature. 2018;

9. Schosserer M, Grillari J, Breitenbach M. The dual role of cellular senescence in developing tumors and their response to cancer therapy. Front. Oncol. 2017.

10. Cheung P, Xiol J, Dill MT, Yuan WC, Panero R, Roper J, et al. Regenerative Reprogramming of the Intestinal Stem Cell State via Hippo Signaling Suppresses Metastatic Colorectal Cancer. Cell Stem Cell. 2020;27.

11. Lukin DJ, Carvajal LA, Liu WJ, Resnick-Silverman L, Manfredi JJ. p53 promotes cell survival due to the reversibility of its cell-cycle checkpoints. Mol Cancer Res. 2015;

12. Saleh T, Tyutyunyk-Massey L, Gewirtz DA. Tumor cell escape from therapy-induced senescence as a model of disease recurrence after dormancy. Cancer Res. 2019;

13. Xu M, Pirtskhalava T, Farr JN, Weigand BM, Palmer AK, Weivoda MM, et al. Senolytics improve physical function and increase lifespan in old age. Nat Med. 2018;

14. Cho YH, Ro EJ, Yoon JS, Mizutani T, Kang DW, Park JC, et al. 5-FU promotes stemness of colorectal cancer via p53-mediated WNT/β-catenin pathway activation. Nat Commun. 2020;

15. Mani SA, Guo W, Liao MJ, Eaton EN, Ayyanan A, Zhou AY, et al. The Epithelial-Mesenchymal Transition Generates Cells with Properties of Stem Cells. Cell. 2008;

16. Liu M, Sakamaki T, Casimiro MC, Willmarth NE, Quong AA, Ju X, et al. The canonical NF-κB pathway governs mammary tumorigenesis in transgenic mice and tumor stem cell expansion. Cancer Res. 2010;

17. Rajasekhar VK, Studer L, Gerald W, Socci ND, Scher HI. Tumour-initiating stem-like cells in human prostate cancer exhibit increased NF-κB signalling. Nat Commun. 2011;

18. Kagoya Y, Yoshimi A, Kataoka K, Nakagawa M, Kumano K, Arai S, et al. Positive feedback between NF-κB and TNF-α promotes leukemia-initiating cell capacity. J Clin Invest. 2014;

19. Nusse YM, Savage AK, Marangoni P, Rosendahl-Huber AKM, Landman TA, De Sauvage FJ, et al. Parasitic helminths induce fetal-like reversion in the intestinal stem cell niche. Nature. 2018;

20. Yui S, Azzolin L, Maimets M, Pedersen MT, Fordham RP, Hansen SL, et al. YAP/TAZ-Dependent Reprogramming of Colonic Epithelium Links ECM Remodeling to Tissue Regeneration. Cell Stem Cell. 2018;

21. Mustata RC, Vasile G, Fernandez-Vallone V, Strollo S, Lefort A, Libert F, et al. Identification of Lgr5-Independent Spheroid-Generating Progenitors of the Mouse Fetal Intestinal Epithelium. Cell Rep. 2013;

22. Marisa L, de Reyniès A, Duval A, Selves J, Gaub MP, Vescovo L, et al. Gene Expression Classification of Colon Cancer into Molecular Subtypes: Characterization, Validation, and Prognostic Value. PLoS Med. 2013;

23. Jorissen RN, Gibbs P, Christie M, Prakash S, Lipton L, Desai J, et al. Metastasis-associated gene expression changes predict poor outcomes in patients with Dukes stage B and C colorectal cancer. Clin Cancer Res. 2009;

24. Cortazar AR, Torrano V, Martín-Martín N, Caro-Maldonado A, Camacho L, Hermanova

I, et al. Cancertool: A visualization and representation interface to exploit cancer datasets. Cancer Res. 2018;

25. Fischer M. Census and evaluation of p53 target genes. Oncogene. 2017.

26. Guinney J, Dienstmann R, Wang X, de Reyniès A, Schlicker A, Soneson C, et al. Guinney et al. 2015. Nat Med. 2015;

27. Lee HO, Hong Y, Etlioglu HE, Cho YB, Pomella V, Van den Bosch B, et al. Lineage-dependent gene expression programs influence the immune landscape of colorectal cancer. Nat Genet. 2020;

28. Puig I, Tenbaum SP, Chicote I, Arqués O, Martínez-Quintanilla J, Cuesta-Borrás E, et al. TET2 controls chemoresistant slow-cycling cancer cell survival and tumor recurrence. J Clin Invest. 2018;

29. Beauséjour CM, Krtolica A, Galimi F, Narita M, Lowe SW, Yaswen P, et al. Reversal of human cellular senescence: Roles of the p53 and p16 pathways. EMBO J. 2003;

30. Kreso A, O'Brien CA, Van Galen P, Gan OI, Notta F, Brown AMK, et al. Variable clonal repopulation dynamics influence chemotherapy response in colorectal cancer. Science (80-). 2013;

31. Brown JA, Yonekubo Y, Hanson N, Sastre-Perona A, Basin A, Rytlewski JA, et al. TGF-β-Induced Quiescence Mediates Chemoresistance of Tumor-Propagating Cells in Squamous Cell Carcinoma. Cell Stem Cell. 2017;

32. Weinberg RA. The retinoblastoma protein and cell cycle control. Cell. 1995.

33. Warren JSA, Xiao Y, Lamar JM. YAP/TAZ activation as a target for treating metastatic cancer. Cancers (Basel). 2018.

34. Rehman SK, Haynes J, Collignon E, Brown KR, Wang Y, Nixon AML, et al. Colorectal Cancer Cells Enter a Diapause-like DTP State to Survive Chemotherapy. Cell. 2021;

35. Dai Y, Wang L, Tang J, Cao P, Luo Z, Sun J, et al. Activation of anaphase-promoting complex by p53 induces a state of dormancy in cancer cells against chemotherapeutic stress. Oncotarget. 2016;

36. Pefani DE, Pankova D, Abraham AG, Grawenda AM, Vlahov N, Scrace S, et al. TGF-β Targets the Hippo Pathway Scaffold RASSF1A to Facilitate YAP/SMAD2 Nuclear Translocation. Mol Cell. 2016;

37. Fumagalli A, Oost KC, Kester L, Morgner J, Bornes L, Bruens L, et al. Plasticity of Lgr5-Negative Cancer Cells Drives Metastasis in Colorectal Cancer. Cell Stem Cell. 2020;

38. De Sousa E Melo F, Kurtova A V., Harnoss JM, Kljavin N, Hoeck JD, Hung J, et al. A distinct role for Lgr5 + stem cells in primary and metastatic colon cancer. Nature. 2017;

39. Morral C, Stanisavljevic J, Hernando-Momblona X, Mereu E, Álvarez-Varela A, Cortina C, et al. Zonation of Ribosomal DNA Transcription Defines a Stem Cell Hierarchy in Colorectal Cancer. Cell Stem Cell. 2020;

40. Sato T, Stange DE, Ferrante M, Vries RGJ, Van Es JH, Van Den Brink S, et al. Long-term expansion of epithelial organoids from human colon, adenoma, adenocarcinoma, and Barrett's epithelium. Gastroenterology. 2011;

41. Mulero M, Ferres-Marco D, Islam A, Margalef P, Pecoraro M, Toll A, et al. Chromatin-bound IκBα regulates a subset of polycomb target genes in differentiation and cancer. Cancer Cell. 2013;24.

42. Krueger B, Friedrich T, Förster F, Bernhardt J, Gross R, Dandekar T. Different evolutionary modifications as a guide to rewire two-component systems. Bioinform Biol Insights. 2012;

43. Langmead B, Salzberg SL. Fast gapped-read alignment with Bowtie 2. Nat Methods. 2012;

44. Zhang Y, Liu T, Meyer CA, Eeckhoute J, Johnson DS, Bernstein BE, et al. Model-based analysis of ChIP-Seq (MACS). Genome Biol. 2008;

45. Yu G, Wang LG, He QY. ChIP seeker: An R/Bioconductor package for ChIP peak annotation, comparison and visualization. Bioinformatics. 2015;

46. Kim D, Pertea G, Trapnell C, Pimentel H, Kelley R, Salzberg SL. TopHat2: Accurate alignment of transcriptomes in the presence of insertions, deletions and gene fusions. Genome Biol. 2013;

47. Anders S, Pyl PT, Huber W. HTSeq-A Python framework to work with high-throughput sequencing data. Bioinformatics. 2015;

48. Love MI, Huber W, Anders S. Moderated estimation of fold change and dispersion for RNA-seq data with DESeq2. Genome Biol. 2014;

49. Galili T, O'Callaghan A, Sidi J, Sievert C. Heatmaply: An R package for creating interactive cluster heatmaps for online publishing. Bioinformatics. 2018;

Acknowledgments: We want to thank the Bigas' and Espinosa's lab members for constructive discussions and suggestions and technical support. We thank our patients for their generosity and to MARbiobank and the IdiPAZ Biobank integrated in the Spanish Hospital Biobanks Network (RetBioH; www.redbiobancos.es).

Funding:

1. Instituto de Salud Carlos III FEDER (PI16/00437 and PI19/00013)
2. Generalitat de Catalunya 2017SGR135
3. PID2019-104867RB-I00/AEI/10.13039/501100011033 funded by the Agencia Estatal de Investigación and the "Xarxa de Bancs de tumors sponsored by Pla Director d'Oncologia de Catalunya (XBTC)
4. Fundación HNA to A.V. research team in the development of orthoxenografts/PDOX.
5. Instituto de Salud Carlos III-Fondo Europeo de Desarrollo Regional (CIBERONC; CB16/12/00244, CB16/12/00241 and CB16/12/00273).
6. IdiPAZ Biobank is supported by Instituto de Salud Carlos III, Spanish Health Ministry (Grant RD09/0076/00073) and Farmaindustria through the Cooperation Program in Clinical and Translational Research of the Community of Madrid.

7. LS is supported by AGAUR (2018 FI_B 00088/2020 FI_B2 00150)
8. A.Ba and T.L-J by a contract from CIBERONC (ISCIII-Feder).
9. T.C-T was funded by the Instituto de Salud Carlos III-FSE (MS17/ 00037; PI18/00014).

Author contributions:

Conceptualization: AB, LE
Biochemical assays, in vitro and in vivo experiments: AV, MG, MS, RGR, MMI, IS
Experiments, investigation and evaluation of results: LS, TLJ, AVe, TCT, AM
Big data analysis and statistical analysis: TLJ, YG, ELA, FT
Clinicopathological characterization of human tumors: MG, RS, CM.
Clinical advice: MG, RS, CM
Writing – original drat: LE, AB
Writing -review & editing: all authors

Competing interests: Authors declare that they have no competing interests.

Data and materials availability: All data associated with this study are present in the paper or the Supplementary Materials. RNA sequencing and ChIP sequencing data have been deposited in NCBI's Gene Expression and are accessible through GEO Series accession no. GSE155354 and no. GSE164161, respectively

FIGURE LEGENDS

Figure 1. Low-dose CT treatment induces a non-senescent quiescent-like state to CRC PDO in the absence of persistent DNA damage.

(A) Dose-response assay of PDO5 treated with 5-FU+Iri. for 72 hours, indicating the IC_{20} and IC_{30} doses. **(B and C)** Quantification of PDO5 **(B)** viability and **(C)** diameter, after 72 hours of 5-FU+Iri. treatment and subsequent washout and culture in fresh medium for 1 and 2 weeks. Representative data from 4 independent experiments is shown. **(D)** Representative images (upper panel) of ki67 staining by immunofluorescence (IF) in PDO5 tumoroid treated with 5-FU+Iri. at IC_{20} and IC_{30} for 72 hours, and quantification (lower panel) of the percentage of $ki67^{+}$ cells/sphere in each condition. Counterstained with DAPI. **(E)** Quantification of SA-β-Gal activity detected by flow cytometry in PDO5 cells treated as in (D). Representative data from 2 independent experiments is shown. **(F)** Dose-response curves of PDO5 treated with the senolytic drug dasatinib for 3 days after pre-treatment with 5-FU+Iri. at the indicated doses for 72 hours. **(G)** Comet assay to measure levels of DNA damage in PDO5 treated for 3 hours as indicated. **(H)** Western blot (WB) analysis of the DNA damage sensor γH2A.X in control and 5-FU+Iri.-treated PDO5 cells collected at the indicated time points after treatment. **(I and J)** Comet assay to measure levels of DNA damage in **(I)** 53 WT PDO5 and **(J)** p53 mutants PDO4 and PDO8, treated for 72 hours as indicated.

The statistical analysis in (D), (G), (I) and (J) was performed by one-way ANOVA test, comparing treated with untreated condition and treated conditions with each other. p values are indicated as *p<0.05 and ****p < 0.0001. n.s., no significant; 5-FU, 5-fluorouracil; Iri, irinotecan; SA-β-Gal, SA-β-Galactosidase; CT, control; IC_{20}, IC_{30} and IC_{60}, 5-FU+Iri. treatment that results in 20%, 30% and 60% cell death, respectively, compared with untreated cell growth.

Figure 2. PQL phenotype is associated with acquisition of a fetal intestinal stem cell (feISC) signature.

(A) Barplot depicting the normalized enrichment score of the statistically significant enriched pathways obtained by GSEA analysis with the Hallmark gene set for treated samples (NOM p-val<0.05). **(B)** WB analysis of control and treated PDO5 cells collected at the indicated time points after 5-FU+Iri. treatment. **(C)** RT-qPCR analysis of selected p53 target genes from control and IC_{20}-treated PDO5 cells. **(D)** GSEA of an intestinal stem cell (ISC) gene set, according to Muñoz et al, in treated versus IC_{20}-treated PDO5 condition. **(E)** Heat map showing the expression levels of the indicated ISC genes in untreated, IC_{20} and IC_{30}-treated PDO5 cells. **(F and G)** GSEA of **(F)** a fetal down and **(G)** a fetal up stem cell gene set, according to Mustata et al, in control (C) versus treated (T) PDO5 condition.

The statistical analysis in (C) was performed by T-Student test, comparing treated with untreated condition. p values are indicated as *p<0.05, **p < 0.01 and ****p < 0.0001. n.s., no significant; CT, control; IC_{20} and IC_{30}, 5-FU+Iri. treatment that results in 20% and 30% cell death, respectively, compared with untreated cell growth; GSEA, gene set enrichment analysis; NES, normalized enriched score.

Figure 3. CT-induced quiescent cells display a fetal intestinal stem cell signature that is p53 dependent.

(A) Expression correlation matrix from the 28up+8down-feISC gene signature using the Marisa database (*n*=566). The size of circles and color intensity are proportional to the Pearson correlation coefficient found for each gene pair. **(B)** RT-qPCR analysis of normalized relative expression of selected 28up+8down-feISC signature genes in control and treated PDO5 as indicated. **(C)** WB analysis of the indicated antibodies in control and treated PDO5 cells collected at the indicated time points after 5-FU+Iri. treatment. **(D, E and F)** RT-qPCR analysis of normalized relative expression of selected 28up-feISC signature genes plus CDKN1A gene in **(D)** control and CT-treated *TP53* WT PDO66, **(E)** *TP53* mutant PDO4 and **(F)** PDO5 *TP53* KO #3. **(G)** WB analysis of various CRC cell lines untreated or collected after 72 hours of 5-FU+Iri. treatment. Membranes were incubated with the indicated antibodies. **(H)** Pie charts showing the molecular subtype distribution (percentage), according to Guinney et al, in patients within the feISC signature groups as indicated. **(I)** Localization of several 28up-fetal-ISC genes in epithelial subtypes cell states 1-9 previously classified in Lee et al 2020. The *t*-SNE plots were obtained using the web-based tool URECA (User-friendly InteRface tool to Explore Cell Atlas). Cell states 1, 5 and 6 correspond to a transcriptional group enriched for secretory and migratory gene expression, whereas cell states 2, 3, 4, 7, 8 and 9 correspond to transport and Wnt signaling gene expression (27).

The statistical analysis in (B), (D), (E) and (F) was performed by T-Student test, comparing treated with untreated condition. p values are indicated as *p<0.05, **p < 0.01 and ****p < 0.0001. n.s., no significant. CT, control; IC_{20} and IC_{30}, 5-FU+Iri. treatment that results in 20% and 30% cell death, respectively, compared with untreated cell growth.

Figure 4. *TP53* WT PQL cells retain tumor-initiating capacity in vitro and in vivo.

(A and B) Number of PDOs (upper panels) and diameter measurement (lower panels) of (**A**) *TP53* WT PDO5 and **(B)** *TP53* mutant PDO4 and PDO8 treated with 5-FU+Iri. as indicated and seeded at 300 cells/well as single cells and after 2 weeks with fresh medium. **(C)** In vivo bioluminescence representative images of mice administered intracardiac injection of 40.000 luciferase-PDO5 CT and IC_{20} or IC_{30} -treated cells in NSG mice. **(D)** Percentage of healthy and with metastasis mice at week 15 from (C). **(E)** Kaplan-Meier representation of disease-free survival probability over time for untreated, IC_{20} and IC_{30}-treated PDO inoculated intracardiac in mice. **(F, G and H) (F)** Number of intraperitoneal implants, **(G)** tumor weight of in situ growing tumors and intraperitoneal implants and **(H)** photographs of tumors derived from orthotopically implanted CT, IC_{20} and IC_{30}-pretreated PDOs in nude mice. **(I)** Immunohistochemistry (IHC) analysis of Ki67 in PDO-derived in situ tumors and implants and quantification of the percentage of $Ki67^+$ tumor cells in the indicated conditions.

The statistical analysis in (A), (B) and (I) was performed by one-way ANOVA test comparing treated with untreated conditions and treated conditions with each other. The statistical analysis

in (F) and (G) by T-Student test, comparing treated with untreated condition. p values are indicated as *p<0.05 and **p < 0.01. n.s., no significant; 5-FU, 5-fluorouracil; Iri, irinotecan; DFS, disease-free survival; IC_{20} and IC_{30}, 5-FU+Iri. treatment that results in 20% and 30% growth reduction, respectively, compared with untreated cell growth.

Figure 5. Identification of a fetal ISC signature with prognosis value in CRC. (A) Cluster analysis of the 28up+8down-feISC signature used to classify patients into at least two subsets in the Marisa colorectal cancer database. We allowed unsupervised hierarchical clustering of the 28+8 genes, while we enforced the classification of patients into 4 subsets (colored in red, green, light blue and purple). Positive and negative correlation expression levels is shown in red and blue, respectively. **(B)** Kaplan-Meier representation of disease-free survival probability over time for patients unclassified and with high or low expression of the 28up+8down-feISC signature selected according to (A) for Marisa colorectal cancer database (28up=high/8down=low *n*=66, 28up=low/8down=high *n*=114 and Unclassified *n*=385). Jorissen (28up=high/8down=low *n*=114 and 28up=low/8down=high *n*=112) and TCGA (28up=high/8down=low *n*=39, 28up=low/8down=high *n*=96 and Unclassified *n*=194) colorectal cancer databases were selected according to their cluster analysis of the 28up+8down-feISC signature. **(C, D and E)** Kaplan–Meier curves representing the disease-free survival probability over time for patients classified according to their cluster analysis of the 28up+8down-feISC signature of patient groups from **(C)** stage II (28up=high/8down=low *n*=23 and 28up=low/8down=high *n*=126), **(D)** stage II and III (28up=high/8down=low *n*=100 and 28up=low/8down=high *n*=368) and **(E)** stage IV (28up=high/8down=low *n*=25 and 28up=low/8down=high *n*=35), from Marisa colorectal cancer database. **(F)** Kaplan-Meier representation of disease-free survival probability over time of patents classified according to their *TP53* status in the Marisa colorectal cancer dataset (*TP53* WT n=161 and *TP53* MUT n=190). **(G)** Kaplan-Meier representation of disease-free survival probability over time of patients, from the Marisa dataset, classified according to their cluster analysis of the 28up+8down-feISC signature for patient groups from *TP53* WT (28up=high/8down=low *n*=27 and 28up=low/8down=high *n*=58) and *TP53* mutant (28up=high/8down=low *n*=6 and 28up=low/8down=high *n*=14). **(H)** Kaplan-Meier representation of disease-free survival probability over time of Marisa patient's tumors previously categorized as CMS4 (26), and classified according to their cluster analysis of the 28up+8down-feISC signature (28up=high/8down=low *n*=23 and 28up=low/8down=high *n*=68). **(I)** Kaplan-Meier representation of disease-free survival probability over time for patients with high or low expression of the 5up+3down-feISC signature of stage III (5up=high/3down=low *n*=17 and 5up=low/3down=high *n*=156) and stage II and III (5up=high/3down=low *n*=87 and 5up=low/3down=high *n*=382) Marisa database, selected according to their unsupervised hierarchical cluster analysis.

Data in (A) show normalized, centered and scaled Illumina probe set intensities on a $\log_2$ scale. The stage lane represents the stage subtype that corresponds to each patient. For statistical

analysis of the Kaplan-Meier estimates we used Cox proportional hazards models (See Supplementary Table S4). HR, hazard ratio.; p, p-value. See also **Figure S5**.

Figure 6. Acquisition of feISC by CT treatment is dependent on YAP1 activation. **(A)** WB analysis of the indicated antibodies of control and *TP53-depleted* PDO5 KO# 3 cells collected after 72 hours of 5-FU+Iri. treatment. **(B)** WB analysis of *TP53* WT (HCT116 and Ls174T) and *TP53* mutant (SW480 and HT29-M6) CRC cell lines untreated and collected after 72 hours of 5-FU+iri. treatment. **(C)** Representative images of YAP1 and the proliferation marker ki67 staining by IF in tumors derived from orthotopically implanted CT, IC_{20} and IC_{30}-pretreated PDOs in nude mice. White arrows indicate nuclear translocation of YAP1. Counterstained, DAPI. **(D)** IHC analysis of YAP1 in representative type 1 (#14) and type 2 (#3, #42) colorectal tumor samples from the same patient at diagnosis (biopsy) and after neoadjuvant therapy at the time of surgery (post-neoadjuvancy). We classified patients based on ki67 levels in the tumor at diagnosis and at surgery. Complete results are shown in Supplementary Table S6. **(E)** Representative images of YAP1 and the fetal gene S100A4 by IF in type 1 (#24) and type 2 (#58) colorectal tumor samples (post-neoadjuvancy). **(F)** RT-qPCR analysis of normalized relative expression of selected 28up-feISC signature genes in control and treated PDO5 with 5-FU+Iri. alone or in combination with verteporfin at a final concentration of 0.2 μM. **(G)** Representative stereoscopic images (left panel) of the *TP53* WT PDO5 and *TP53* mutant PDO8 treated with 5-FU+Iri. alone, verteporfin alone or in combination with verteporfin at a final concentration of 1 μM and quantification (right panel) of the relative cell growth in both PDOs treated with verteporfin alone or in combination with 5-FU+Iri. **(H)** Dose-response curves of IC_{20}-pretreated PDO5 treated for 3 days as indicated.

Statistical analysis in (F) was performed by T-Student test, comparing treated with untreated conditions and treated conditions with each other. p values are indicated as *$p<0.05$, **$p < 0.01$, n.s., no significant. CT, control; IC_{20} and IC_{30}, 5-FU+Iri. treatment that results in 20% and 30% cell death, respectively, compared with untreated cell growth.

FIGURES

Fig.1.

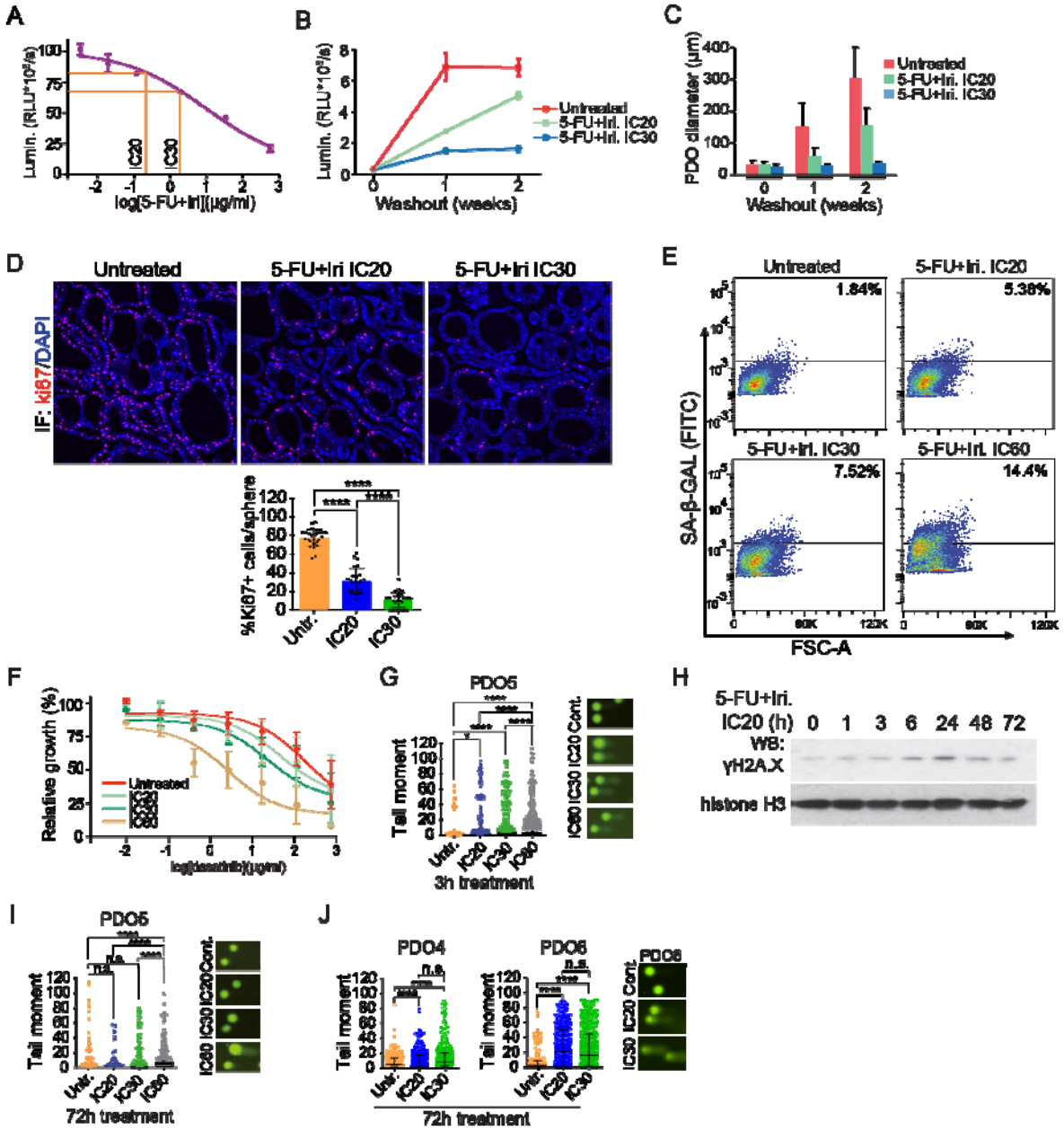

943 **Fig.2.**

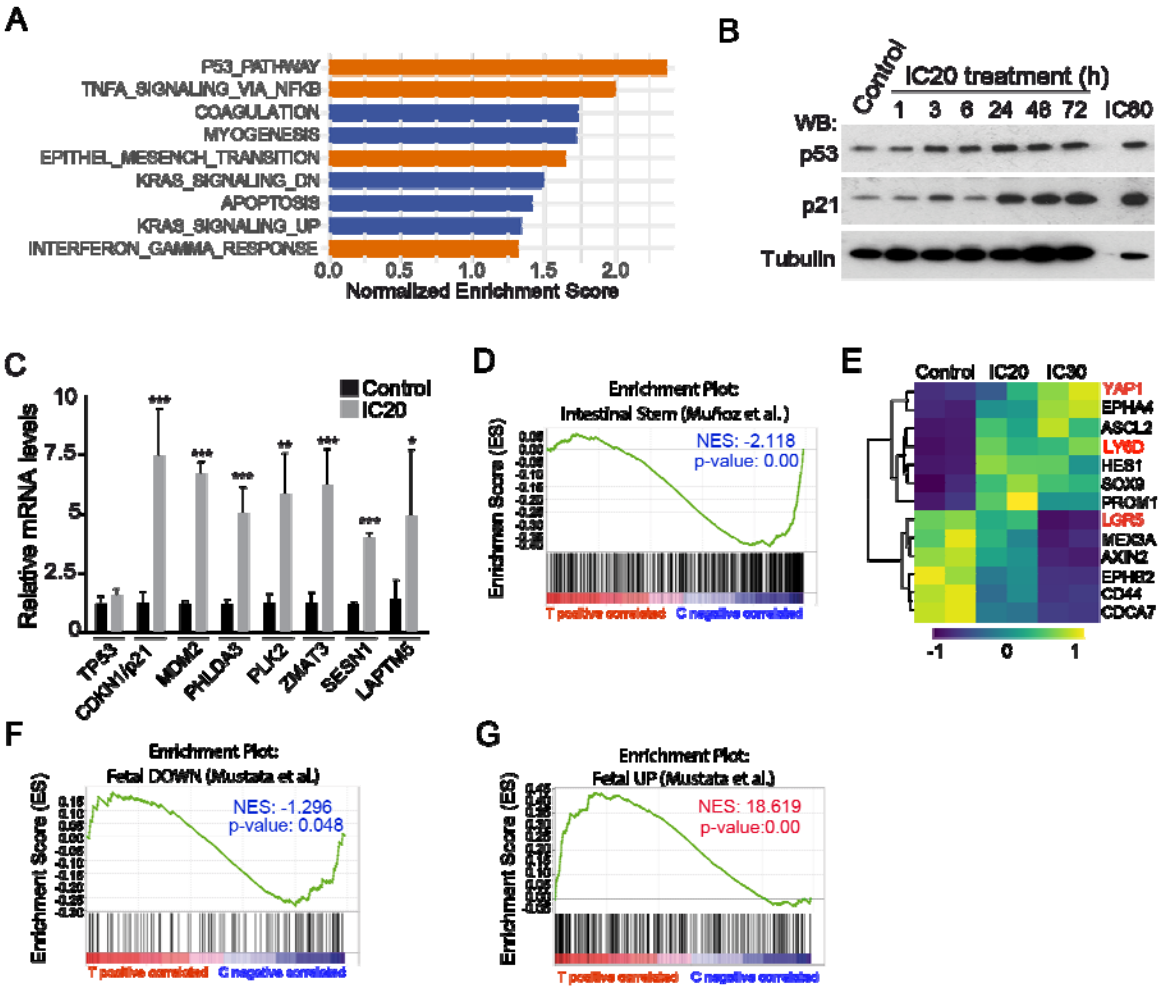

944
945
946
947
948
949
950
951
952
953

Fig.3.

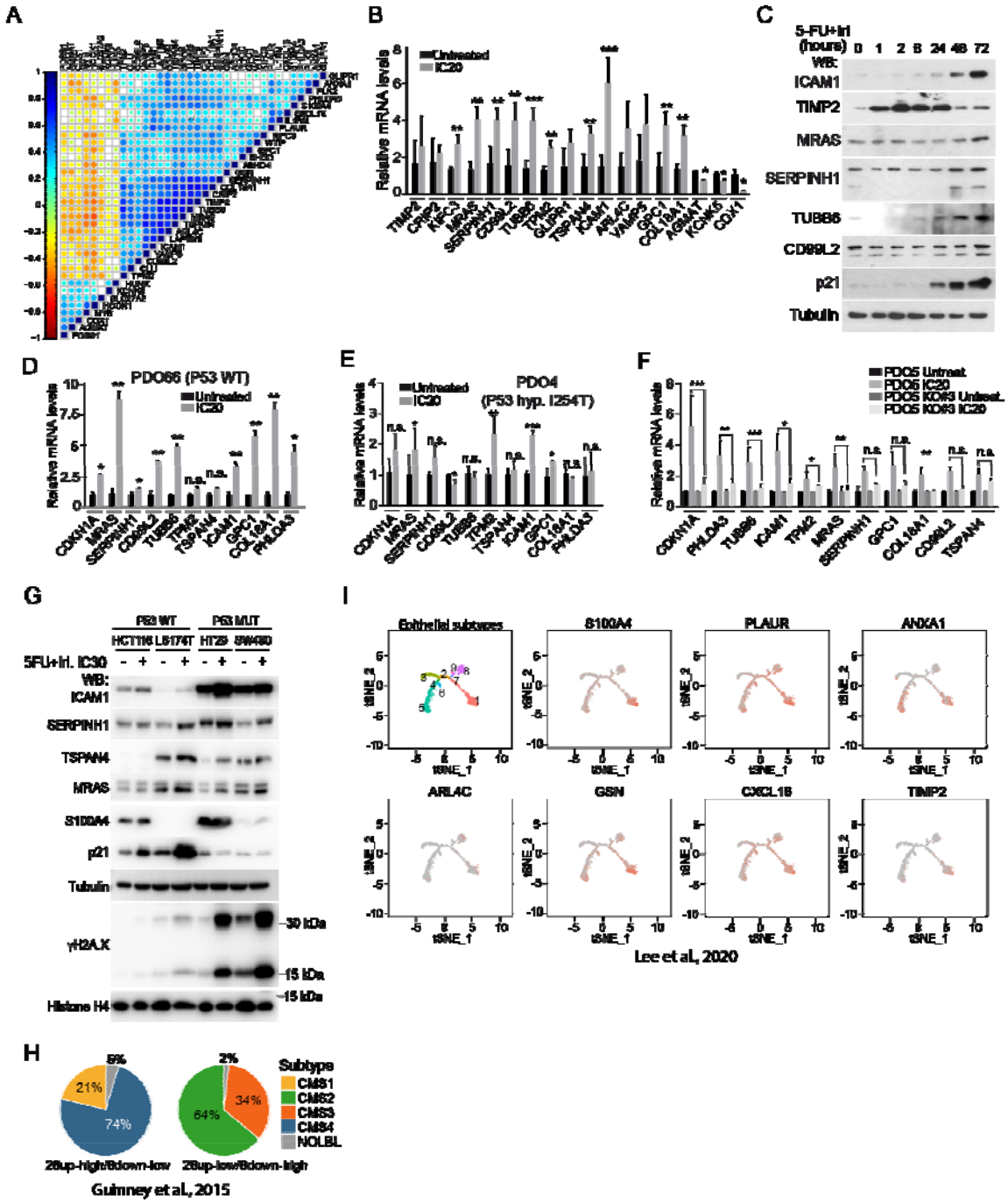

962 **Fig.4.**

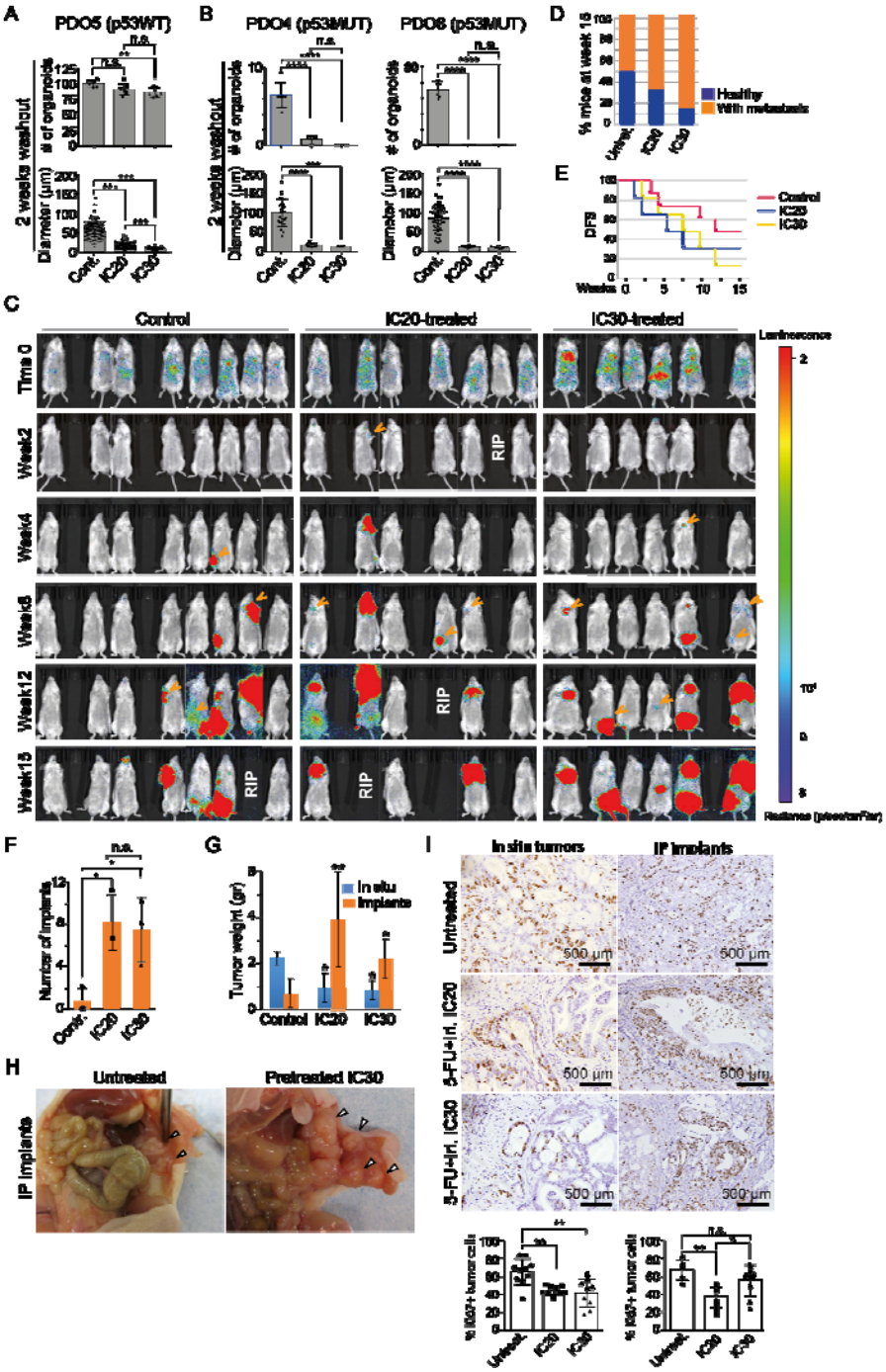

963

964

965

966

967

968 **Fig.5.**

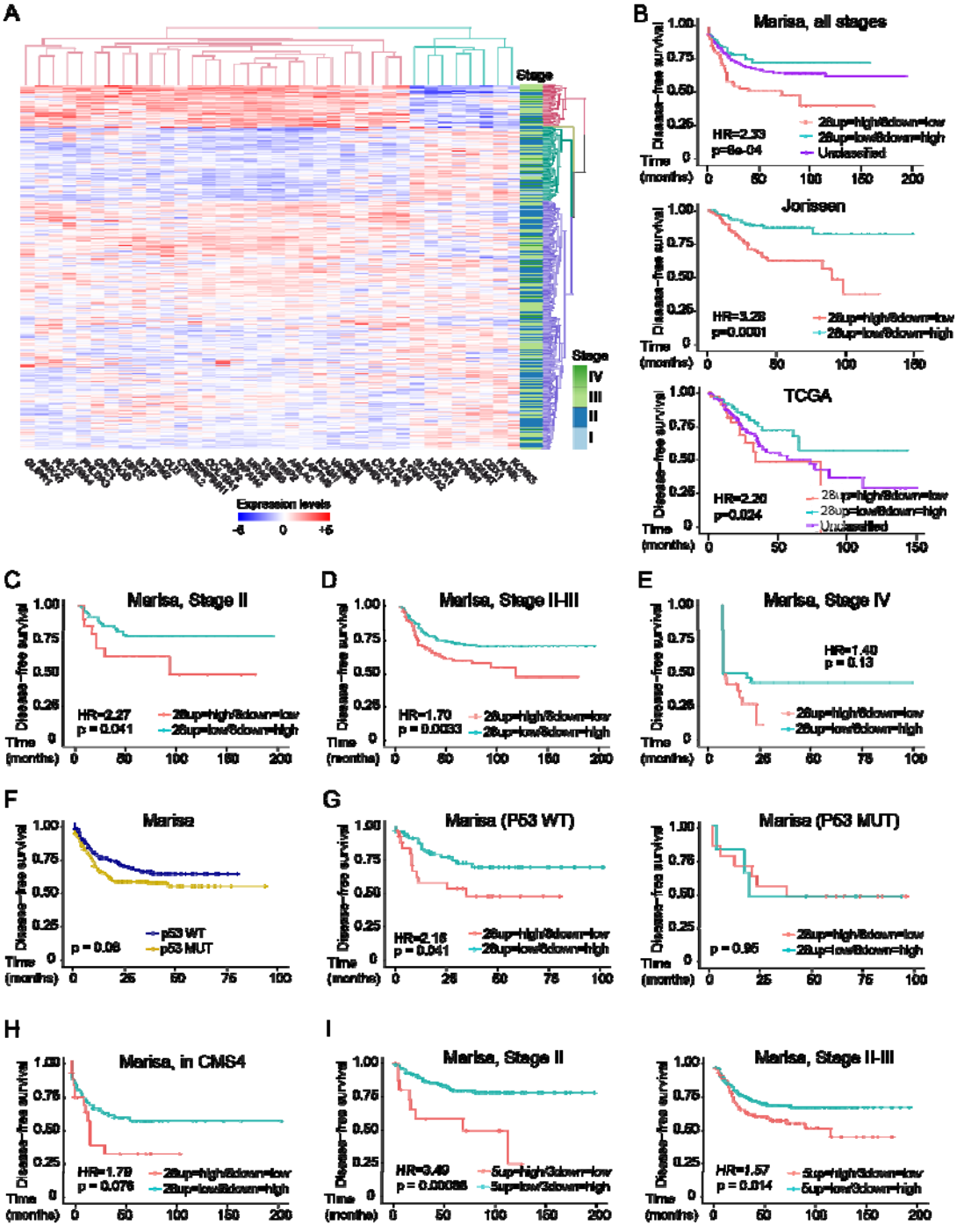

969

970

971

Fig.6.

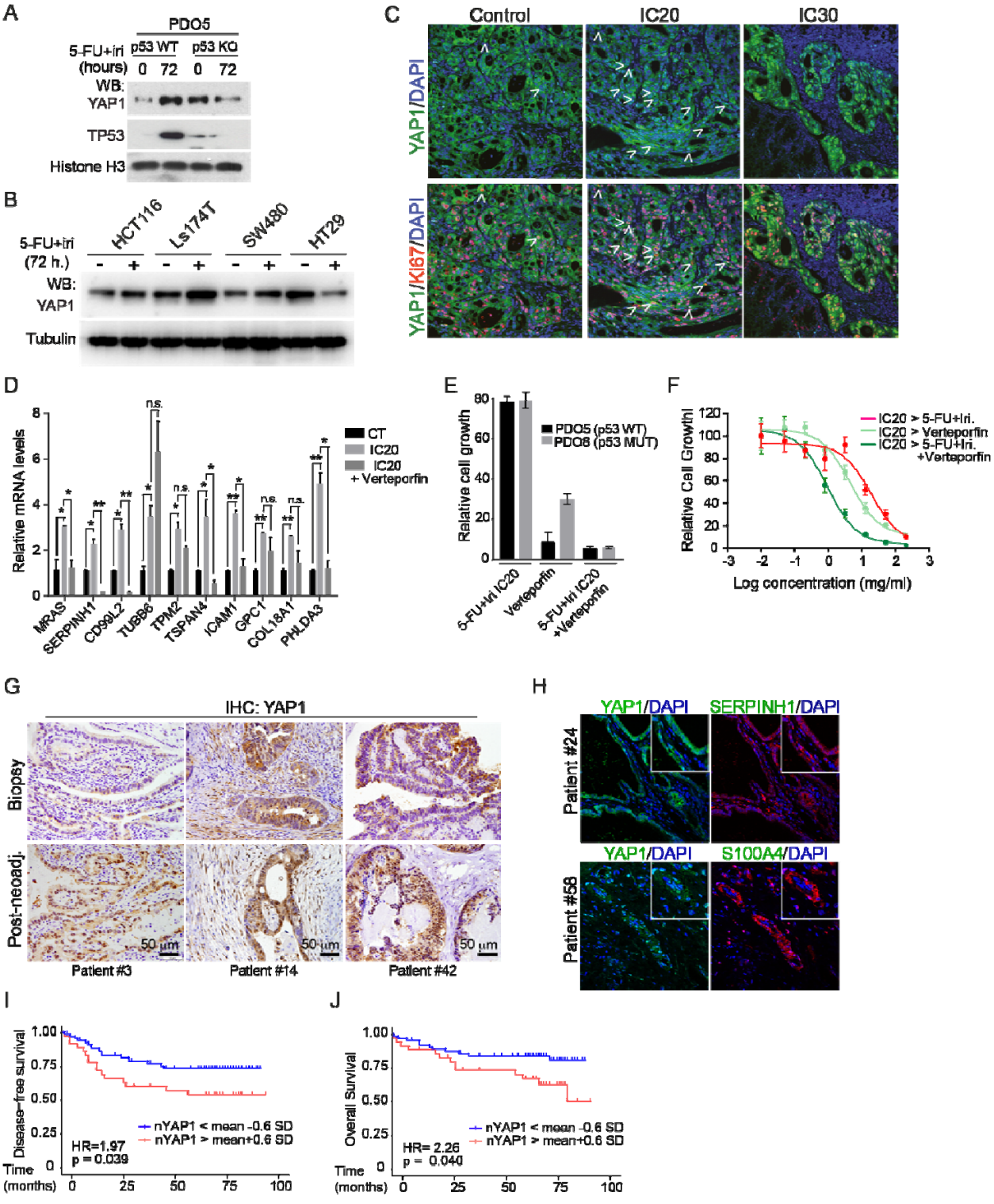

977

978

Supplementary materials and methods:

Immunohistochemical staining

Paraffin blocks were obtained from tissues and PDOs, previous fixation in 4% formaldehyde overnight at room temperature. Paraffin-embedded sections of 4 µm, for tissues, and 2.5 µm, for PDOs, were de-paraffinized, rehydrated and endogenous peroxidase activity was quenched (20 min, 1.5% H_2O_2). EDTA or citrate□based antigen retrieval was used depending on the primary antibody used. All primary antibodies were diluted in PBS containing 0.05% BSA, incubated overnight at 4 °C and developed with the Envision+ System HRP Labelled Polymer anti-Rabbit or anti-Mouse and 3,3′-diaminobenzidine (DAB). Samples were mounted in DPX and images were obtained with an Olympus BX61 microscope.

Immunofluorescence analysis

For tissues and PDOs, the same protocol as IHC was followed. However, the samples were developed with Tyramide Signal Amplification System (TSA) and mounted in DAPI Fluoromount-G. Images were taken in an SP5 upright confocal microscope (Leica).

Hematoxylin and eosin staining

Previously de-paraffinized sections were incubated with hematoxylin 30 s, tap water 5 min, 80% ethanol 0.15% HCl 30 s, water 30 s, 30% ammonia water (NH3(aq)) 30 s, water 30 s, 96% ethanol 5 min, eosin 3 s, and absolute ethanol 1 min. Samples were dehydrated, mounted in DPX, and images were obtained with an Olympus BX61 microscope.

FISH

Fluorescent in-situ hybridization (FISH) analyses from control and IC_{30}-treated PDOs were performed using commercial probes (Abbott Molecular Inc, Des Plaines, IL, USA), one including the centromeric alfa-satellite region specific for chromosome 8, and a second one containing locus-specific probes from the long arm of chromosome 13 and 21.

In brief, we performed a cytospin to concentrate nuclei in the FISH slide. Slides were pre-treated with pepsin for 5 minutes at 37ºC. Samples and probe were co-denaturated at 80ºC for five minutes and hybridized overnight at 37ºC in a hot plate (Hybrite chamber, Abbot Molecular Inc.). Post-hybridization washes were performed at 73ºC in 2xsodium salt citrate buffer (SSC) and at room temperature in 2xSSC, 0.1% NP-40 solution. Samples were counterstained with 4,6-diamino-2-phenilindole (DAPI)(Abbott Molecular Inc, Des Plaines, IL, USA). Results were analyzed in a fluorescence microscope (Olympus, BX51) using the Cytovision software (Applied Imaging, Santa Clara, CA). A minimum of 50 nuclei per case was analyzed.

Comet assay

Comet assays were performed using Comet Assay Kit following manufacturer's instructions. Pictures were taken using a Nikon Eclipse Ni-E epifluorescence microscope and tail moment was calculated using the OPENCOMET plugin for Fiji.

Annexin V binding assay

Annexin V binding was determined by flow cytometry using the standard Annexin V Apoptosis Detection Kit APC. Single cells of treated PDOs with indicated combinations of 5-FU+Iri. were obtained and stained according to the manufacturer's instructions, with Propidium Iodide staining for the DNA content. The cells were analyzed in the Fortessa analyzer.

PDO initiating capacity assay

For PDO Initiating Capacity assay, 300 or 600 single PDO cells were plated in 96-well plates in 10 µL Matrigel. After 11 days in culture, the number of PDOs in each well was counted, photographs were taken for PDO diameter determination and cell viability was measured.

Chromatin-immunoprecipitation assay (ChIP)

Control and IC20-treated PDOs were subjected to ChIP following standard procedures. Briefly, PDO cells were extracted with formaldehyde crosslinked for 10 min at room temperature and lysed for 20 min on ice with 500 µL of H_2O plus 10 mM Tris-HCl pH 8.0, 0.25% Triton X-100, 10 mM EDTA, 0.5 mM EGTA, 20 mM β-glycerol-phosphate, 100 mM NA-orthovanadate, 10 mM NaButyrate and complete protease inhibitor cocktail. The supernatants were sonicated, centrifuged at 13.000 rpm for 15 min, and supernatants were incubated overnight with anti-p53 antibody in RIPA buffer. Precipitates were captured with 35 mL of protein A-Sepharose, extensively washed and analysed by ChIP-qPCR. Primers used are listed in Supplementary Table S7. Inputs were used to normalize the ChIP-qPCR and samples were compared to control IgGs.

PDOs infection

hFLiG plasmid was used for in vivo detection of metastasis, H2BeGFP plasmid was used for flow cytometry experiments and lentiCRISPR v2 was used for knock-out experiments. Three sgRNA against *TP53* gene were designed using Benchling (Supplementary Table S7). Lentiviral production was performed transfecting in HEK293T cells the lentiviral vectors and the plasmid of interest. One day after transfection, medium was changed, and viral particles were collected 24 hours later and then concentrated using Lenti-X Concentrator. PDOs were infected by resuspending single cells in concentrated virus diluted in complete medium, centrifuged for 1 h at 650 rcf, and incubated for 5 hours at 37°C. Cells were then washed in complete culture medium and seeded as described above.

Description of the patient gene expression data sets

Transcriptomic and available clinical data datasets from colorectal, breast, prostate and lung cancer were downloaded from the open-access resource CANCERTOOL. For

CRC we used the Marisa (GSE39582) data set, which includes expression and clinical data for 566 patients with CRC and 19 non-tumoral colorectal mucosa, and the Jorissen (GSE14333) data set and the TCGA data set with expression and clinical data of 226 and 329 CRC patients, respectively. For Lung cancer we used the Okayama (GSE31210) data set, which includes expression profiles of 226 lung adenocarcinomas and the TCGA data set with 434 patients.

Association of the signatures with clinical outcome

Association of the signatures expression with relapse was assessed in the cancer transcriptomic data sets using a Kaplan-Meier estimates and Cox proportional hazard models. A standard log-rank test was applied to assess significance between groups. This test was selected because it assumes the randomness of the possible censorship. All the survival analyses and graphs were performed with R using the survival (v.3.2-3) and survimer (v.0.4.8) packages and a p-value<0.05 was considered statistically significant (see Supplementary Table S4).

Supplementary figures and tables:

Fig. S1. Low-dose CT treatment induces a quiescent-like state to CRC PDO in the absence of persistent DNA damage and senescence.

Fig. S2. Low-dose CT induces a robust p53 signaling.

Fig. S3. p53 and p21 dependency of the feISC signature.

Fig. S4. TQL cells retain tumor initiating capacity.

Fig. S5. Identification of a fetal ISC signature with prognostic value in cancer.

Fig. S6. Acquisition of quiescent phenotype by CT treatment in patients.

Table S1. Patient-derived organoids used in this study.

Table S2. Differentially expressed genes between IC20 or IC30 and control PDOs.

Table S3. Expression correlation matrix from CT induced feISC genes in the Marisa (Marisa et al., 2013) dataset.

Table S4. Cox proportional hazards analysis of the feISC signature.

Table S5. Positive correlation of individual genes to the rest of the cohort.

Table S6. Human gastrointestinal tumor samples used in this study.

Table S7. List of oligonucleotides for RT-qPCR and ChIP-qPCR and sgRNA for CIRSPR/Cas9 knockout used in this study.

Table S8. Materials table.

Fig. S1.

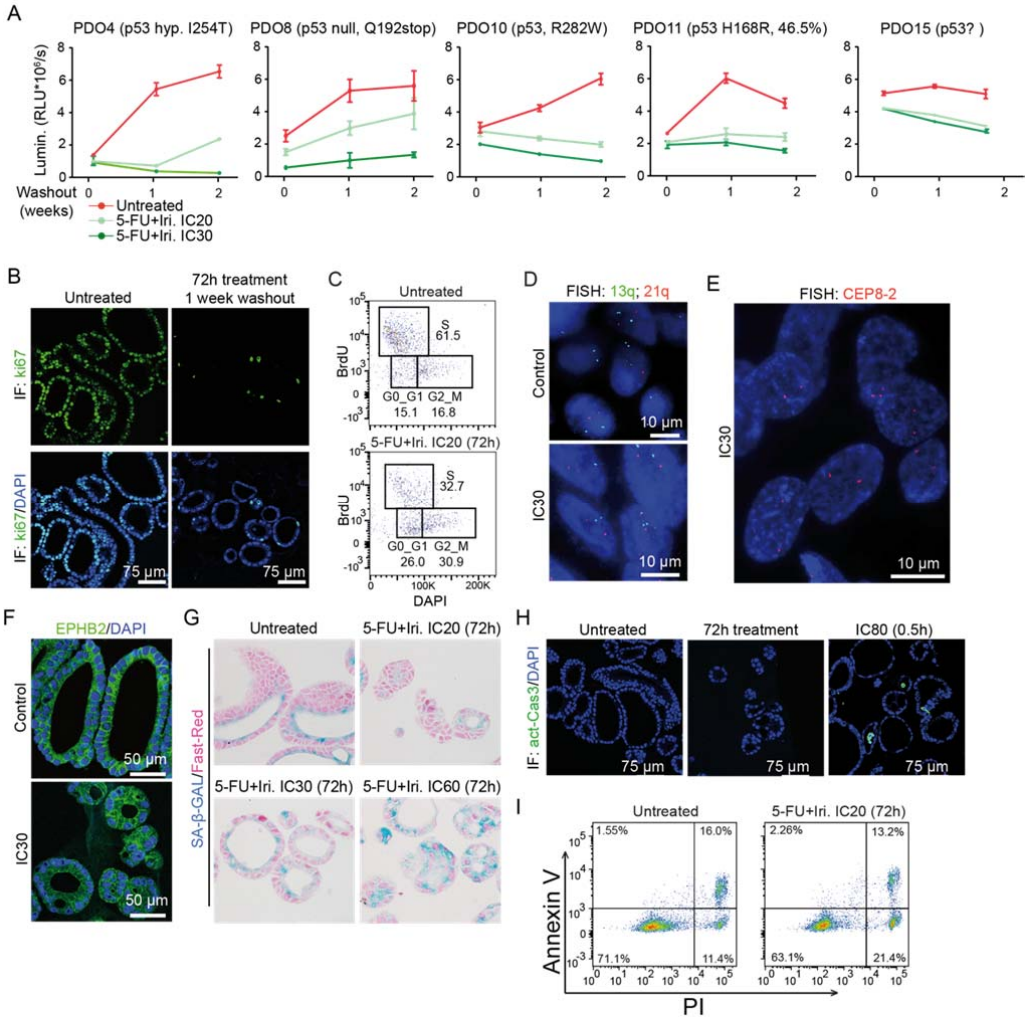

Figure S1. Related to Figure 1. Low-dose CT treatment induces a quiescent-like state to CRC PDO in the absence of persistent DNA damage and senescence.

(A) Quantification of cell viability of the different PDOs untreated or pretreated with 5-FU+Iri. for 72 hours and then maintained in fresh medium for 1 and 2 weeks after washout. **(B)** Representative images of the proliferation marker ki67 staining by IF in PDO5 tumoroid treated with 5-FU+Iri. at IC_{20} for 72 hours and after being maintained in fresh medium for 1 week. **(C)** Flow cytometry analysis showing BrdU incorporation of PDO5 after 72 hours of 5-FU+Iri. treatment, compared with the control. Three boxes are shown, representing cells in G_0/G_1, S and G_2/M cell cycle, respectively. **(D and E)** Representative images of fluorescent in-situ hybridization (FISH) analysis from control and IC_{30}-treated PDO5 using probes for **(D)** 13q (green) and 21q (red) and **(E)** the centromeric probe CEP8-2 (red). **(F)** Representative images of IF analysis using the surface marker EPHB2 in control and IC_{30}-treated PDO5 tumoroid. DAPI is used as a

nuclear marker. **(G)** Analysis of SA-β-Gal activity in PDO5 cells treated with 5-FU+Iri. as indicated for 72 hours. Representative images were obtained with Olympus BX61. **(H)** Representative IF images of cleaved-caspase 3 staining in PDO5 treated with 5-FU+Iri. at IC_{20} at the indicated time points and with IC_{80} as a positive control. **(I)** Cytometry analysis of Annexin V binding in PDO5 untreated or treated as indicated.
SA-β-Gal, SA-β-Galactosidase; 5-FU, 5-fluorouracil; Iri, irinotecan; CT, control; IC_{20} and IC_{30}, 5-FU+Iri. treatment that results in 20% and 30% cell death, respectively, compared with untreated cell growth.

Fig. S2.

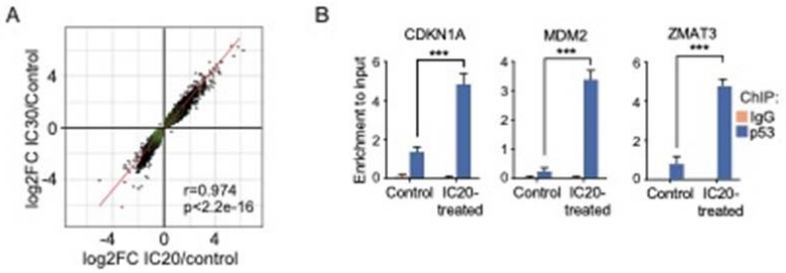

Figure S2. Related to Figure 2. Low-dose CT induces a robust p53 signaling.
(A) Linear association of the genes differentially expressed in treated PDO5 compared with the control. Dots represent the log_2 fold change values of genes for IC_{20} compared with control (x-axis) and IC_{30} compared with control (y-axis). The Pearson correlation and p value are shown. **(B)** ChIP-qPCR analysis of p53 binding in untreated and IC_{20}-treated PDO5 in a subset of putative p53 target genes expressed as relative enrichment normalized to the input.
The statistical analysis in (B) was performed by T-Student test, comparing treated with untreated condition. p values are indicated as ****$p < 0.0001$. CT, IC_{20} and IC_{30}, 5-FU+Iri. treatment that results in 20% and 30% cell death, respectively, compared with untreated cell growth.

Fig. S3.

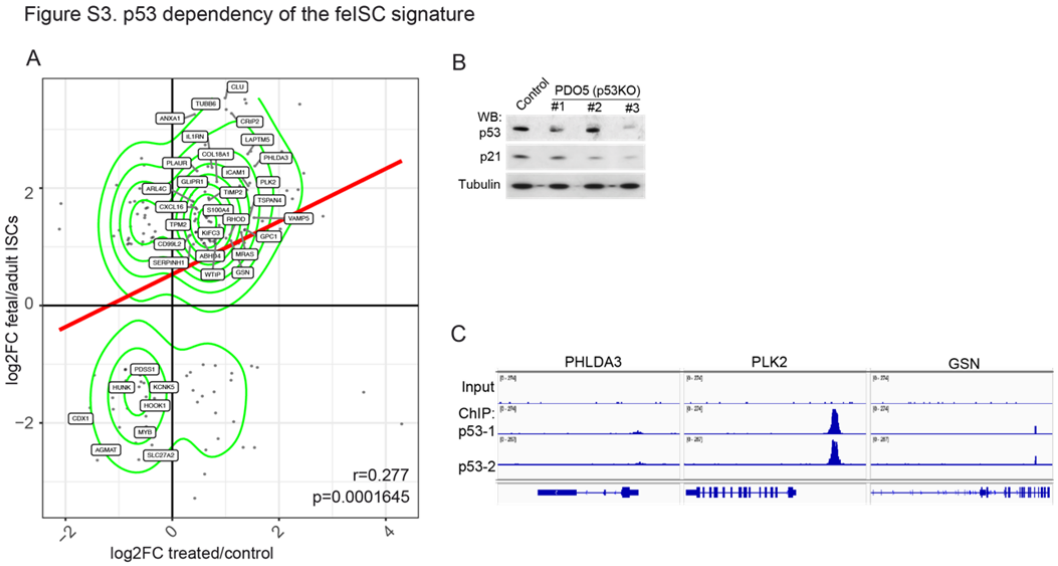

Figure S3. Related to Figure 3. p53 and p21 dependency of the feISC signature.
(A) Scatter plot and linear regression line of the genes differentially expressed between CT treated and control PDOs and fetal compared with adult intestinal stem cell. Dots represent the log2 fold change values of genes for treated versus control (xaxis) and fetal versus adult intestinal stem cell (y-axis). The Pearson correlation and p value are shown. Genes included in the 28up+8down-feISC signature are indicated. **(B)** WB analysis of p53 levels and its downstream target p21 in CRISPR-Cas9-engineered p53 KO pools. **(C)** Representation of some 28up-feISC genes distribution in the indicated genomic regions obtained from ChIP-sequencing analysis in IC_{20}-treated PDO5 (n=2).

Fig. S4.

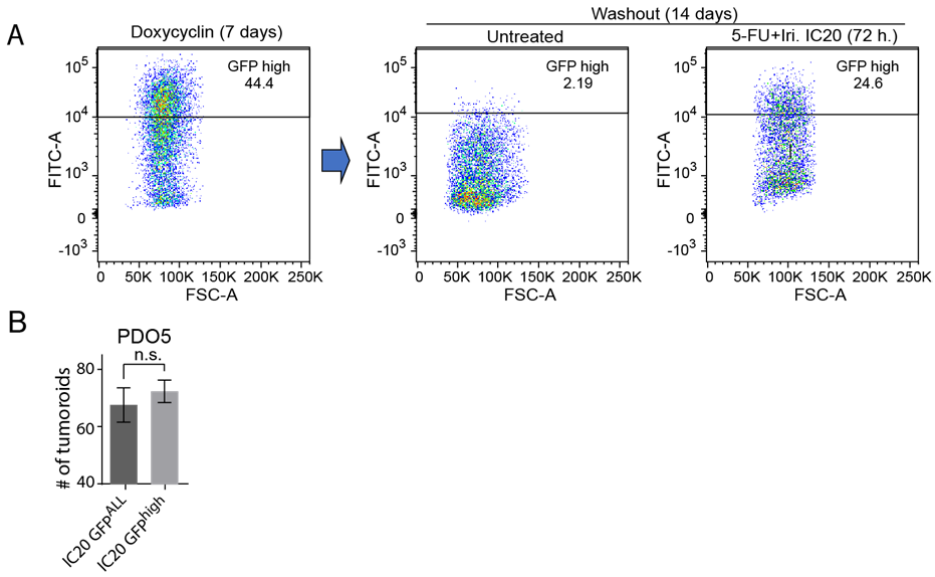

Figure S4. Related to Figure 4. TQL cells retain tumor initiating capacity.

(A) Analysis of GFP distribution by flow cytometry of PDO5 cells carrying a doxycycline-inducible GFP-H2B construct. Cells were treated for 6 days with doxycycline to induce GFP-H2B expression and then left untreated or treated with 5-FU+Iri. IC_{30} for 72 hours and maintained in fresh medium for 2 additional weeks. Quiescent cells that retained high or low GFP levels were purified by cell sorting. **(B)** Number of PDOs generated from seeding 300 $GFP^{high+low}$ and GFP^{high} sorted cells after 2 weeks with fresh medium.

n.s., no significant; IC_{20}, 5-FU+Iri. treatment that results in 20% cell death, compared with untreated cell growth.

Fig. S5.

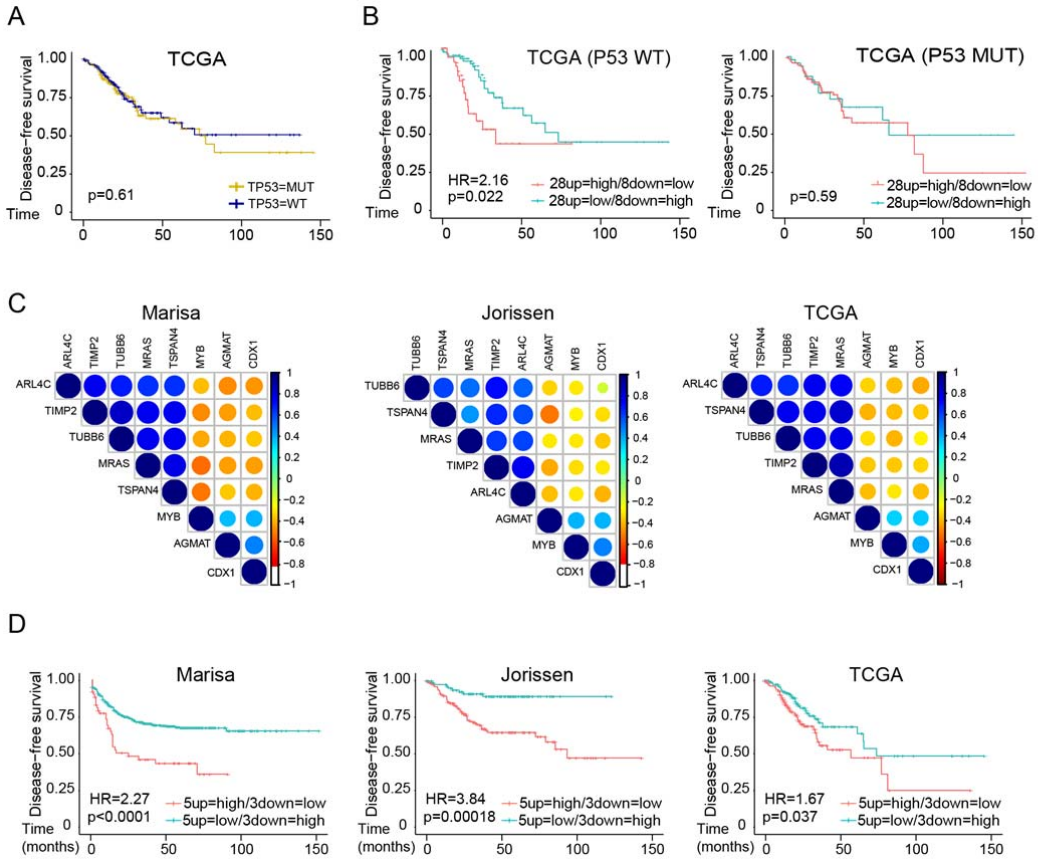

Figure S5. Related to Figure 5. Identification of a fetal ISC signature with prognostic value in cancer.

(**A**) Kaplan-Meier representation of disease-free survival probability over time of patients classified according to their *TP53* status (*TP53* WT n=144 and *TP53* MUT n=177) in the TCGA colorectal cancer dataset. **(B)** Kaplan-Meier representation of disease-free survival probability over time of patients, from the TCGA dataset, classified according to their cluster analysis of the 28up+8down-feISC signature (data not shown) for patient groups from *TP53* WT (28up=high/8down=low *n*=47 and 28up=low/8down=high *n*=97) and *TP53* mutant (28up=high/8down=low *n*=128 and 28up=low/8down=high *n*=49). **(C)** Expression correlation matrix according to the 5up+3down-feISC signature in the Marisa, Jorissen and TCGA datasets. Positive and negative correlation is shown in blue and red, respectively. The size of circles and color intensity are proportional to the Pearson correlation coefficient found for each gene pair. **(D)** Kaplan–Meier curves of disease-free survival probability over time of patients classified according to their cluster analysis of the 28up+8down-feISC signature (data not shown), for Marisa (5up=high/3down=low *n*=59 and 5up=low/3down=high *n*=507), Jorissen (5up=high/3down=low *n*=137 and 5up=low/3down=high *n*=89) and

TCGA (5up=high/3down=low *n*=128 and 5up=low/3down=high *n*=105) colorectal databases.

For statistical analysis of the Kaplan-Meier estimates we used Cox proportional hazards models (See Supplementary Table S4). HR, hazard ratio.; p, p-value.

Fig. S6.

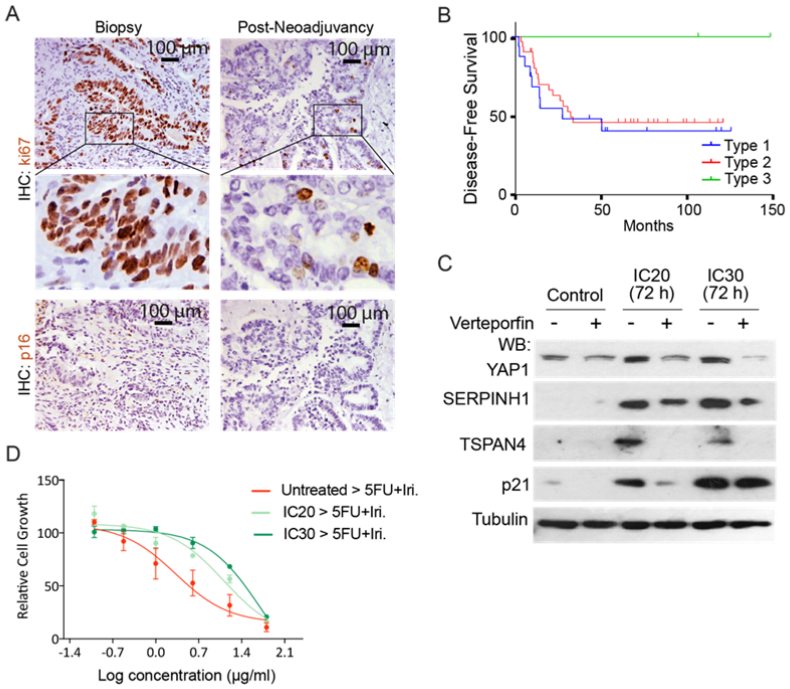

Figure S6. Related to Figure 6. Acquisition of quiescent phenotype by CT treatment in patients. (A) IHC analysis of Ki67 and p16 in representative type 2 colorectal tumor samples (Table S6 #17) from the same patient at diagnosis (biopsy) and after neoadjuvant therapy at the time of surgery (post-neoadjuvancy). (**B**) Disease-free survival analysis (Kaplan-Meier curves) of patients stratified according to ki67-related tumor type. **(C)** WB analysis of control and treated *TP53* WT Ls174T CRC cells collected after 24 hours of 5-FU+Iri. treatment alone or in combination with the YAP1 inhibitor verteporfin at a final concentration of 5 □M. **(D)** Dose-response assay of PDO5 cells untreated or previously treated for 72 hours with IC_{20}-IC_{30} 5-FU+Iri.

Supplementary Table S1. Patient-derived organoids used in this study. The mutations and the corresponding chemotherapy concentrations that reduce a 20 and 30% of the cell growth (IC20 and IC30, respectively) are indicated for each PDO.

PDO	Mutations	IC20 (µg/mL)	IC30 (µg/mL)
PDO4	TP53 I254T (100%) EGFR S464L (97.21%)	5-FU 1.25 Iri. 0.50	5-FU 2.00 Iri. 0.80
PDO5	KRAS G12D (66.43%)	5-FU 0.14 Iri.] 0.06	5-FU 0.25 Iri. 0.10
PDO8	TP53 Q192stop (98.46%) KRAS G13C (67.27%)	5-FU 0.78 Iri. 0.31	5-FU 1.56 Iri. 0.63
PDO10	TP53 R282W (99.82) FGFR2 C809W (62.72%) KRAS A146V (80.25%)	5-FU 6.25 Iri. 2.50	5-FU 12.50 Iri. 5.00
PDO11	TP53 H168R (46.54%) FGFR2 N194stop (45.87%) KRAS G12D (49.58%) ERBB2 A87T (4.76%) PIK3CA S874N (41.93%) PDGFRA R293H (5.97%) EGFR K960R (46.3%) BRAF E71D (42.08%)	5-FU 0.78 Iri. 0.31	5-FU 1.56 Iri. 0.63
PDO15	TP53 G262V (98.82%)	5-FU 1.56 Iri. 0.63	5-FU 3.13 Iri. 1.25
PDO66	NRAS (G12S) (99.05%) APC (S1110stop) (99.80)	5-FU 0.63 Iri. 0.30	5-FU 2.50 Iri. 1.00

Table S4 Cox proportional hazards analysis of the feISC signature. Association of the signature with recurrence-disease free survival. Related to Figure 4 and Figure S4.

Cluster			p value (logrank test)	HR recurrence	lower.95 (HR)	upper.95 (HR)
GSE39582 (Marisa et al) (n=566 patients)						
28up=high/8down=low						
	All stages	*n= 66*	8.00E-04	2.33	1.40	3.9
	Stage II	*n= 23*	4.10E-02	2.27	1.01	5.1
	Stage II-III	*n= 100*	3.30E-03	1.71	1.19	2.5
	Stage IV	*n= 25*	2.37E-01	1.48	0.77	2.8
	p53WT	*n= 27*	4.67E-02	2.16	1.01	4.6
	p53MUT	*n= 6*	9.60E-01	1.04	0.27	4.0
5up=high/3down=low						
	All stages	*n= 59*	3.00E-05	2.27	1.53	3.4
	Stage II	*n= 17*	9.00E-04	3.49	1.60	7.7
	Stage II-III	*n= 87*	2.41E-02	1.57	1.06	2.3
	CMS4	*n= 23*	7.60E-02	1.79	0.92	3.46
TCGA-COAD+READ (TCGA Portal) (n=329 patients)						
28up=high/8down=low						
	All stages	*n= 39*	2.40E-02	2.20	1.09	4.43
	P53WT	*n= 47*	2.10E-02	2.16	1.1	4.20
	P53MUT	*n= 128*	5.90E-02	1.18	0.63	2.21
5up=high/3down=low						
	All stages	*n= 128*	3.70E-02	1.67	1.03	2.72
	P53 WT	*n= 144*	6.08E-01	0.89	0.58	1.37
GSE14333 (Jorissen et al) (n=226 patients)						
28up=high/8down=low						
	All stages	*n= 114*	1.00E-04	3.28	1.74	6.18
5up=high/3down=low						
	All stages	*n= 137*	2.00E-4	3.84	1.80	8.21

5
6

Table S5 Positive correlation of individual genes to the rest of the cohort. Genes within the 5up+3down-feISC signature are highlighted in gray. Related to Figure 5 and S5.

Gene	State	GSE39582 (Marisa et al)	TCGA-COAD+READ (TCGA Portal)	GSE14333 (Jorissen et al)	Final Score
ABHD4	up	9,69	9,39	7,31	26,39
ANXA1	up	9,44	11,85	8,82	30,12
ARL4C	up	13,77	14,96	12,84	41,57
CD99L2	up	9,48	9,65	4,87	23,99
CLU	up	10,84	9,07	9,18	29,09
COL18A1	up	14,22	14,74	10,80	39,76
CRIP2	up	13,76	14,17	9,11	37,04
CXCL16	up	8,12	7,54	8,59	24,25
GLIPR1	up	8,08	9,84	9,18	27,10
GPC1	up	11,18	11,40	8,45	31,03
GSN	up	9,85	11,30	3,41	24,56
ICAM1	up	12,82	13,66	9,16	35,64
IL1RN	up	9,70	9,66	7,92	27,28
KIFC3	up	10,77	14,54	3,25	28,57
LAPTM5	up	13,56	14,90	11,43	39,88
MRAS	up	15,43	16,61	10,53	42,57
PHLDA3	up	11,92	12,29	5,69	29,90
PLAUR	up	11,48	10,39	10,19	32,07
PLK2	up	9,78	10,16	8,90	28,84
RHOD	up	8,63	4,08	7,79	20,50
S100A4	up	11,56	10,19	9,35	31,09
SERPINH1	up	13,66	13,66	10,22	37,53
TIMP2	up	15,72	16,68	13,80	46,21
TPM2	up	11,24	13,25	8,91	33,41
TSPAN4	up	15,69	16,26	12,19	44,15
TUBB6	up	15,37	15,78	11,66	42,81
VAMP5	up	13,26	14,07	7,73	35,06
WTIP	up	8,59	12,75	5,23	26,57
AGMAT	down	3,74	3,21	3,32	10,28
CDX1	down	3,61	3,13	3,37	10,12
HOOK1	down	3,42	2,93	3,12	9,47
HUNK	down	2,73	2,72	2,74	8,18
KCNK5	down	2,60	2,39	2,49	7,48
MYB	down	3,62	3,46	3,50	10,58
PDSS1	down	3,46	2,98	2,42	8,86
SLC27A2	down	2,69	2,12	2,22	7,03

Supplementary Table S6. Human gastrointestinal tumor samples used in this study. Paired samples at diagnosis (biopsy) and after neoadjuvant therapy at the time of surgery (postQ). The corresponding clinical data, ki67 subtype classification and presence of nuclear YAP1 is indicated.

Relapse
0. Regression
1. Local recurrence
2. Metastasis

Status
1. Alive without disease
2. Alive with disease
3. Dead without disease
4. Dead with disease

ki67 subtype
1. No changes in ki67 levels
2. Decrease in ki67 levels
3. Decrease in ki67 levels displaying giant nuclei

Patient nº	Tumor Localization	Clinical TNM	Treatment	ki67% postQ	ki67% biopsy	ki67 subtype	nuclear YAP1% postQ	nuclear YAP1% biopsy	OS (mo)	DFS (mo)
1	Gastric	T4N1M1	Chemotherapy	20	40	2	30	0	7,13	5,40
2	Colorectal	T3N1M1	Chemotherapy + Targeted therapy	1	55	3	N/A	N/A	115,23	115,23
3	Gastric	T3N1	Chemotherapy	10	70	2	90	5	60,90	60,90
4	Colorectal	T3N1M1	Radiotherapy	5	70	2	N/A	N/A	17,33	9,50
5	Gastric	T3N1M0	Chemotherapy	5	60	2	80	5	26,73	12,23
6	Colorectal	T3N0	Chemotherapy	30	70	2	50	2	53,10	53,10
7	Gastric	T3N1M1	Chemotherapy	70	90	2	90	80	41,10	23,07
8	Gastric	T3N1M1	Chemotherapy + Targeted therapy	10	5	1	70	0	89,83	40,23
9	Colorectal	T3N1	Chemotherapy	15	75	2	N/A	N/A	94,23	94,23
10	Gastric	T3N0M0	Chemotherapy	85	95	1	5	10	91,10	91,10
11	Gastric	T2-3N1M0	Chemotherapy	90	90	1	N/A	N/A	93,37	93,37
12	Gastric	T3N1M0	Chemotherapy	80	90	1	N/A	N/A	97,70	97,70
13	Gastric	T3N0M0	Chemotherapy	20	70	2	0	0	25,23	9,67
14	Colorectal	T4N1	Chemotherapy	80	60	1	95	20	38,17	12,43
15	Gastric	T3N1M1	Chemotherapy + Targeted therapy	70	85	1	50	15	93,37	93,37
16	Colorectal	T3N1	Chemotherapy + Targeted therapy	10	80	2	90	0	42,67	21,67
17	Colorectal	T4N1M0	Chemotherapy	20	95	2	60	20	39,90	39,90
18	Colorectal	T3N0M0	Chemotherapy	40	90	2	N/A	N/A	81,53	81,53
19	Colorectal	T2N1M0	Chemotherapy	5	25	3	90	3	83,13	83,13
20	Colorectal	T4N1M0	Chemotherapy	20	60	2	70	60	94,03	94,03
21	Colorectal	T3N1M0	Chemotherapy	25	80	2	N/A	30	91,90	91,90
22	Colorectal	T3N1M0	Chemotherapy	1	95	2	N/A	N/A	88,30	88,30
23	Colorectal	T3N2bM0	Chemotherapy	1	90	2	30	30	76,53	76,53
24	Gastric	T3N1M0	Chemotherapy	20	20	1	90	0	29,87	12,77
25	Colorectal	T3N1M0	Chemotherapy	N/A	N/A	N/A	N/A	N/A	79,77	N/A
26	Colorectal	T3N0M0	Chemotherapy	N/A	N/A	N/A	N/A	N/A	53,63	N/A
27	Colorectal	T3N0M0	Chemotherapy	1	55	2	5	10	8,53	8,53
28	Colorectal	T3N1M0	Chemotherapy + Targeted	40	65	2	30	1	121,23	27,47

			therapy							
29	Colorectal	T3N1M0	Chemotherapy	N/A	N/A	N/A	N/A	N/A	33,90	20,83
30	Colorectal	T3N0	Chemotherapy	20	10	1	70	3	60,30	60,30
31	Gastric	T3N0	Chemotherapy	20	30	1	100	0	12,17	9,10
32	Gastric	T3N1	Chemotherapy	30	40	1	N/A	N/A	16,53	8,40
33	Gastric	T3N0M0	Chemotherapy	30	70	2	80	5	77,93	77,93
34	Colorectal	T3N1M1	Chemotherapy + Targeted therapy	5	80	2	90	0	N/A	N/A
35	Colorectal	T3N1M0	Radiotherapy	1	60	2	100	15	69,50	69,50
36	Gastric	T3N1M0	Chemotherapy	25	N/A	N/A	N/A	N/A	39,37	39,37
37	Gastric	T3N1M0	Chemotherapy	20	55	2	2	2	65,10	65,10
38	Gastric	T3N1M0	Chemotherapy	10	20	1	60	20	39,23	22,73
39	Pancreas	T4N0M0	Chemotherapy	0	N/A	N/A	N/A	N/A	45,63	15,63
40	Colorectal	T3N1M1	Chemotherapy	25	30	1	90	10	18,23	6,00
41	Colorectal	T3N0M0	Radiotherapy	25	40	1	30	0	41,77	41,77
42	Colorectal	T3N0M1	Chemotherapy + Targeted therapy	40	90	2	90	0	22,50	10,13
43	Colorectal	T4N1M0	Chemotherapy	0	65	2	0	5	45,60	11,90
44	Colorectal	T3N1	Chemotherapy	5	15	1	0	5	8,70	8,70
45	Colorectal	T3N0M0	Chemotherapy	1	70	2	N/A	N/A	62,73	25,00
46	Colorectal	T3N1M1	Chemotherapy + Targeted therapy	5	50	2	80	0	33,47	18,43
47	Colorectal	T3N2M0	Chemotherapy	60	95	2	0	2	59,63	26,40
48	Colorectal	T3N1M0	Chemotherapy	20	60	2	30	0	56,20	56,20
49	Gastric	T4N0M0	Chemotherapy	50	60	1	50	50	42,70	42,70
50	Colorectal	T3N0M0	Chemotherapy	10	70	2	5	0	47,60	47,60
51	Gastric	T2N1M0	Chemotherapy	15	75	2	2	0	38,73	16,70
52	Colorectal	T3N0M0	Chemotherapy	5	25	2	30	0	63,37	63,37
53	Colorectal	T3N1M0	Chemotherapy	20	95	2	30	0	9,00	9,00
54	Gastric	T3N3M0	Chemotherapy	15	60	2	30	0	11,93	11,03
55	Colorectal	T4N1M0	Radiotherapy	20	30	1	15	0	34,73	34,73
56	Colorectal	T2N1M0	Chemotherapy	N/A	N/A	N/A	N/A	N/A	53,27	N/A
57	Colorectal	T3N1M0	Chemotherapy	45	85	2	50	5	54,47	54,47
58	Colorectal	T3N0M0	Chemotherapy	70	90	2	90	20	50,67	50,67
59	Colorectal	T3N0M0	Chemotherapy	45	80	2	70	25	12,23	5,00
60	Colorectal	T4N2M0	Chemotherapy	75	95	2	40	0	22,47	4,27
61	Colorectal	T3Nx (sigma)+ T2N0 (rectum) M1	Radiotherapy	65	65	1	N/A	N/A	36,47	3,27
62	Colorectal	T3N0 (rectum) + T4Nx (bladder) M1	Radiotherapy	80	95	1	80	5	5,37	3,53

Supplementary Table S7. List of oligonucleotides for RT-qPCR and ChIP-qPCR and sgRNA for CIRSPR/Cas9 knockout used in this study.

Primers for RT-qPCR		
Target	**Forward**	**Reverse**
TP53	CTTTGAGGTGCGTGTTTGTG	GGGCAGTGCTCGCTTAGT
CDKN1A	CCGAAGTCAGTTCCTTGTGGA	TGGTGTCTCGGTGACAAAGT
MDM2	GCCATTGAACCTTGTGTGATT	GGCAGGGCTTATTCCTTTTC
PHLDA3	CAGCTGTGGAAGCGGAAG	GCGAAGCTGAGCTCCTTG
PLK2	AATAACAAAGTCTACGCCGCA	TCTTTGTCAATCTTTTCCCTTTG
ZMAT3	CTAGGGCAAAGCGCAAATAG	GACCAGCCACTCCAAAAGAG
SESN1	TGACCTGATGCCTTTCCTTC	CCTGGGGCTTAGTACCTTCC
LAPTM5	TCTTTTCCATCGCCTTCATC	CCTTCTGGAGCATCTTGGAG
TIMP2	TTCCCTCCCTCAAAGACTGA	CAAAGCCACCTACCTCCAAA
CRIP2	CGGTGGGCAGCTACATCTAT	CTGAGCACTCTCCCAGCAGA
KIFC3	TGCCATGTACGAGTCAGAGC	CGGTTCTTGTCCTCTTCCAG
MRAS	ACCGAGTTTTCCCATCAGTG	TCTCTTTCCCTCCCAGGTTT
SERPINH1	CTTCATGGTGACTCGGTCCT	CGATTTGCAGCTTTTCCTTC
CD99L2	CGGGTTGACATGAGAAAGGT	ATTCTGGCTTTGATGCTCGT
TUBB6	TGAGGGGCCACAAAATAAAC	TATAAGGCAACACGGCACAA
TPM2	GGACAGAGGATGAGGTGGAA	GCATCAGTGGCCTTCTTCTC
GLIPR1	CGCCATCACAAACTGGTATG	ATCTGCCCAAACAACCTGAG
TSPAN4	TGCCTCCTGCTCACTTTCTT	GTCTTGCTGGGCATACCTGT
ICAM1	GAAGTGGCCCTCCATAGACA	TCAAGGGTTGGGGTCAGTAG
ARL4C	TGAGTCCCTGCCTATTGTCC	CAGATGGGCTGCTAGGTTTC
VAMP5	CCTGAAGGAGAAGCCAAATG	GTCAAGGGAGAGCAAACACC
GPC1	CCCTACGCTCATCTCTGGAA	GACCTTGTGGAGGAAGGACA
COL18A1	GAGGGACAAGTGGACTCAGG	TTGGCTTCACATCACACACA
AGMAT	TCTTTCTGGGAACACAGCCC	CGGTTGTCACTTTGGGGAGA
KCNK5	GAGGTGTGAGTCTGCGGAAG	GCCCTCGATGTAGTTCCACC
CDX1	ACCTCCTCTCCAATGCCTGT	AGACTCGGACCAGACCTCCT
HPRT1	ATAAGCCAGACTTTGTTGG	ATAGGACTCCAGATGTTTCC
TBP	GGAAGTGACATTATCAACGC	CCAAGAAACAGTGATGCTG
ACTB	GCACCACACCTTCTACAATGAGC	TAGCACAGCCTGGATAGCAACG
Primers for ChIP-qPCR		
Target	**Forward**	**Reverse**
MDM2	GGGCAGGTTGACTCAGCTTTT	AGCTGGGAAAATGCATGGTTTA
BAX	GGTTCCTGGCTCTCTGATCC	AGGCTGGGCCTGTATCCTAC
CDKN1A	AGCAGGCTGTGGCTCTGATT	CAAAATAGCCACCAGCCTCTTCT
ZMAT3	CAAATTGCCACAAACATTCTGC	CTGGGGGAGACACATGCTAGA
sgRNA for CRISPR/Cas9 knockout		
Target	**sgRNA sequence**	
TP53 – Guide 1	TCGACGCTAGGATCTGACTG	
TP53 – Guide 2	ACCAGCAGCTCCTACACCGG	
TP53 – Guide 3	CCATTGTTCAATATCGTCcG	

1 **Table S8. Materials table**

2

REAGENT or	SOURCE	IDENTIFIER
Antibodies		
Mouse monoclonal anti-γH2AX (pS139)	BD Biosciences	Cat#564719; RRID:AB_2738913
Mouse monoclonal anti-Ki67 (MM1)	Leica Biosystems	Cat#NCL-Ki67-MM1; RRID:AB_442101
Rabbit polyclonal anti-Cleaved Caspase-3 (Asp175)	Cell Signaling	Cat#9661; RRID:AB_2341188
Mouse monoclonal anti-p53 DO-1	Abcam	Cat#ab1101; RRID:AB_297667
Rabbit monoclonal anti-p21 [EPR362]	Abcam	Cat#ab109520; RRID:AB_10860537
Rabbit monoclonal anti-CKN2A/p16INK4a [EPR1473]	Abcam	Cat#ab108349; RRID:AB_10858268
Goat polyclonal anti-EphB2	RD Systems	Cat#AF467; RRID:AB_355375
Rabbit polyclonal anti-CD99L2	Abcam	Cat#ab224164
Mouse monoclonal anti-TIMP2 [3A4]	Abcam	Cat#ab1828; RRID:AB_2256129
Rabbit polyclonal anti-MRas	Abcam	Cat#ab26303; RRID:AB_470849
Anti-TUBB6	Abcam	Cat#PA5-P8948
Recombinant Anti-ICAM1 antibody [EPR4776]	Abcam	Cat#ab109361; RRID:AB_10958467
Recombinant Anti-Hsp47 antibody [EPR4217]	Abcam	Cat#ab109117; RRID:AB_10888995
Recombinant Anti-YAP1 antibody [EP1674Y]	Abcam	Cat#ab52771; RRID:AB_2219141
TSPAN4 Polyclonal Antibody	Thermo Fisher Scientific	Cat#PA5-69344; RRID:AB_2688603
Monoclonal Anti-S100A4 antibody produced in mouse	Atlas Antibodies	Cat#AMAB90599; RRID:AB_2665603
Anti-Histone H3 antibody-Nuclear Marker and ChIP Grade	Abcam	Cat#ab791; RRID:AB_302613

Anti-Histone H4 antibody–ChIP Grade	Abcam	Cat#ab10158; RRID:AB_296888
Mouse monoclonal anti-alpha-Tubulin (B-5-1-2)	Sigma-Aldrich	Cat#T6074; RRID:AB_477582
Goat Anti-Rabbit Immunoglobulins/HRP antibody (2ary)	Agilent	Cat#P0448; RRID:AB_2617138
Rabbit Anti-Mouse Immunoglobulins/HRP antibody (2ary)	Agilent	Cat#P0260; RRID:AB_2636929
Polyclonal Rabbit Anti-Goat Immunoglobulins/HRP antibody (2ary)	Agilent	Cat#P0449; RRID:AB_2617143
Biological Samples		
Patient-derived organoids (PDO): PDO4, PDO5, PDO8, PDO10, PDO11, PDO15	Hospital del Mar (Barcelona)	MARBiobanc (https://marbiobanc.imim.es)
Patient-derived organoids (PDO): PDO66	From Alberto Muñoz Lab (Fernández-Barral et al., 2020)	RetBioH (www.redbiobancos.es)
Human gastrointestinal tumors blocks	Hospital del Mar (Barcelona)	MARBiobanc (https://marbiobanc.imim.es)
Chemicals, Peptides, and Recombinant Proteins		
Collagenase II from *Clostridium histolyticum*	Sigma-Aldrich	Cat#C6885
Hyaluronidase from bovine testes	Sigma-Aldrich	Cat#H3506
DMEM/F-12 Advanced	GIBCO	Cat#12634028
Primocin	Invitrogen	Cat#ant-pm-1
B-27 Supplement (50X)	GIBCO	Cat#17504044
N-2 supplement (100X)	GIBCO	Cat#17502048
Nicotinamide	Sigma-Aldrich	Cat#N3376
N-Acetyl-L-cysteine	Sigma-Aldrich	Cat#A7250

Recombinant Human Noggin	PeproTech	Cat#120-10C
Recombinant Human R-Spondin-1	PeproTech	Cat#120-38
Y-27632 dihydrochloride (ROCK inhibitor)	Sigma-Aldrich	Cat#Y0503
Prostaglandin E2	Tocris	Cat#2296
SB 202190	Sigma-Aldrich	Cat#S7067
A8301 (ALK inhibitor)	Sigma-Aldrich	Cat#SML0788
hEGF	Sigma-Aldrich	Cat#E9644
Gastrin I (human)	Tocris	Cat#3006
Corning Matrigel Basement Membrane Matrix, LDEV-free	Corning	Cat#354234
5-Fluorouracil (5-FU)	Accord Healthcare	Cat#606544.3
Irinotecan	Accord Healthcare	Cat#713386.5
Dasatinib	Selleckchem	Cat#S1021
Verteporfin	Selleckchem	Cat#S1786
D-Luciferin	Goldbio	Cat#LUCK
PhosSTOP phosphatase inhibitor cocktail	Roche	Cat#PHOSS-RO
cOmplete Mini protease inhibitor cocktail	Roche	Cat#11836170001
DPX mountant	Sigma-Aldrich	Cat#06522
DAPI Fluoromount-G	Southern Biotech	Cat#0100-20
Protein A-Sepharose CL-4B	GE Healthcare	Cat#17-0780-01
Protein G-Sepharose 4 Fast Flow	GE Healthcare	Cat#17-0618-01

Critical Commercial Assays		
Dako Envision+ System-HRP Labelled Polymer anti-Rabbit	Agilent	Cat#K4003
Envision+ System-HRP Labelled Polymer anti-Mouse	Agilent	Cat#K4001
Dako Liquid DAB+ Substrate Chromogen System	Agilent	Cat#K3468
TSA Plus Cyanine 3/Fluorescein System	PerkinElmer	Cat#NEL753001KT
EZ-ECL Chemiluminescence Detection Kit for HRP	Biological Industries	Cat#20-500-120
ECL Prime Western Blotting System	GE Healthcare	Cat#RPN2232
CellTiter-Glo Luminescent Cell Viability Assay	Promega	Cat#G7571
APC BrdU Flow Kit	BD Biosciences	Cat#552598
Senescence β-Galactosidase Staining Kit	Cell Signaling	Cat#9860S
Cell Event Senescence Green Flow Cytometry Assay KiT	Invitrogen	Cat#C10840
CometAssay Kit	Trevigen	Cat#4250-050-K
RNeasy Micro Kit	Qiagen	Cat#74004
RT-First Strand cDNA Synthesis Kit	GE Healthcare Life Sciences	Cat#27-9261-01
SYBR Green I Master Kit	Roche	Cat#04887352001
Annexin V Apoptosis Detection Kit APC	Invitrogen	Cat#88-8007
Lenti-X Concentrator	Clontech	Cat#631232
Experimental Models: Cell Lines		

Human: HEK293T	ATCC	CRL-11268
Human: HCT116	ATCC	CCL-247
Human: Ls174T	ATCC	CL-188
Human: SW480	ATCC	CCL-228
Human: HT29	ATCC	HTB-38D
Experimental Models: Organisms/Strains		
Mouse: NU/J (*Foxn1*^{nu})	The Jackson Laboratory	JAX: 002019
Oligonucleotides		
Primers for RT-qPCR, see Table S7	This study	N/A
Primers for Chip-qPCR, see Table S7	This study	N/A
gRNA against *TP53*, see Table S7	This study	N/A
Recombinant DNA		
Plasmid: pMD2.G	From Trono Lab, unpublished	Addgene plasmid #12259
Plasmid: pCMV-dR8.2 dvpr	Stewart et al., 2003	Addgene plasmid #8455
Plasmid: lentiCRISPR v2	Sanjana et al., 2014	Addgene plasmid #52961
Plasmid: pLEX-hFLiG	Celià-Terrassa & Kang, 2018	N/A
Plasmid: pLTPC-H2BeGFP	Gift from Héctor G. Palmer Lab, unpublished	N/A
Software and Algorithms		
GraphPad Prism 6	Graphpad Software	https://www.graphpad.com; RRID:SCR_002798
Fiji (Image J)	Schneider et al., 2012	https://www.fiji.sc; RRID: SCR_002285
Benchling CRISPR design	Benchling	https://www.benchling.com; RRID: SCR_013955
FlowJo 10.6.2	BD Biosciences	https://www.flowjo.com; RRID: SCR_008520

LightCycler Software	Roche	http://www.roche-applied-science.com/shop/products/absolute-quantification-with-the-lightcycler-carousel-based-system; RRID: SCR_012155
Adobe Photoshop	Adobe Software	https://www.adobe.com/products/photoshop.html; RRID: SCR_014199
RStudio	RStudio Team	https://rstudio.com/
GSEA	Broad Institute	https://www.gsea-msigdb.org/gsea/index.jsp
ggplot	Bioconductor	
Corrplot	CRAN	https://cran.r-project.org/web/packages/corrplot/index.html
Survimer	CRAN	https://CRAN.R-project.org/package=survminer
Survival	CRAN	https://CRAN.R-project.org/package=survival
Heatmaply	CRAN	https://CRAN.R-project.org/package=heatmaply
Pheatmap	CRAN	https://CRAN.R-project.org/package=pheatmap
Limma	Bioconductor	https://bioconductor.org/packages/release/bioc/html/limma.html
DESeq2 R package	Bioconductor	https://bioconductor.org/packages/release/bioc/html/DESeq2.html
TopHat	Kim et al 2013	https://ccb.jhu.edu/software/tophat/index.shtml
HTSeq	Anders et al. 2015	https://htseq.readthedocs.io/en/master/